A constitutive scaling law and a unified comprehension for frictional slip failure, shear fracture of intact rock, and earthquake rupture

Mitiyasu Ohnaka[1]

Earthquake Prediction Research Center, Earthquake Research Institute, University of Tokyo, Tokyo, Japan

Received 22 December 2000; revised 23 November 2001; accepted 16 August 2002; published 7 February 2003.

[1] It is widely recognized that some of the physical quantities inherent in a rupture are scale-dependent, and the scale dependence is one of the most notable facts and features of rupture phenomena. The paper addresses how such scale-dependent shear rupture of a broad range from laboratory-scale frictional slip failure and shear fracture of intact rock to field-scale rupture as an earthquake source can be unified by a single constitutive law. Noting that the earthquake rupture is a mixed process between frictional slip failure and the shear fracture of intact rock, it is concluded that the constitutive law for the earthquake rupture be formulated as a unifying law that governs both frictional slip failure and shear fracture of intact rock. It is demonstrated that the slip-dependent constitutive law is such a unifying law, and a constitutive scaling law is derived from laboratory data on both frictional slip failure and shear fracture of intact rock. This constitutive scaling law enables one to provide a consistent and unified comprehension for scale-dependent physical quantities inherent in the rupture, over a broad range from small-scale frictional slip failure and shear fracture in the laboratory to large-scale earthquake rupture in the field. *INDEX TERMS:* 5104 Physical Properties of Rocks: Fracture and flow; 7209 Seismology: Earthquake dynamics and mechanics; 7260 Seismology: Theory and modeling; 8010 Structural Geology: Fractures and faults; 8020 Structural Geology: Mechanics; *KEYWORDS:* unified constitutive formulation, constitutive scaling law, inhomogeneous fault surfaces, characteristic length scale, physical scaling relation

Citation: Ohnaka, M., A constitutive scaling law and a unified comprehension for frictional slip failure, shear fracture of intact rock, and earthquake rupture, *J. Geophys. Res.*, *108*(B2), 2080, doi:10.1029/2000JB000123, 2003.

1. Introduction

[2] Rupture (or fracture) phenomena, including the earthquake rupture, are observed in a very broad range from an atomistic scale, through a microscopic scale, to a macroscopic scale. Laboratory-scale rupture, including the shear fracture of intact materials and frictional slip failure on a preexisting fault, may roughly be of the order of 10^{-3} to 1 m, whereas field-scale rupture, including micro- to large earthquakes, may be of the order of 10^{-1} to 10^{5} m. In this paper, focus is placed on the shear rupture in the range from laboratory-scale to field-scale that continuum mechanics encompasses.

[3] It is widely recognized that some of the physical quantities inherent in the rupture are scale-dependent, and the scale-dependence is one of the most notable facts and features of rupture phenomena. The scale-dependent physical quantities include the shear rupture energy [*Aki*, 1979, 1984], the breakdown zone size, the nucleation zone size, and the slip acceleration [e.g., *Ohnaka and Shen*, 1999; *Ohnaka*, 2000]. In particular, the shear rupture energy has the dimensions of energy per unit area; nevertheless, it is scale dependent (see later sections). For instance, it has been estimated by seismologists [e.g., *Aki*, 1979, 1984; *Papageorgiou and Aki*, 1983] that the shear rupture energy for major earthquakes is in the range 10^{6}–10^{8} J/m^2. In contrast, laboratory experiments show that the shear fracture energy of intact granite samples under lithospheric conditions is in the range 10^{4}–10^{5} J/m^2 [*Wong*, 1982a, 1986; *Ohnaka et al.*, 1997]. As noted by *Aki* [1979, 1984], therefore, there is a distinct difference in the amount of the fracture energy between large-scale earthquake rupture in the field and small-scale shear fracture in the laboratory. In spite of these facts, many scientists still believe that the shear rupture energy cannot be scale-dependent because it should be material constant. This is a paradox to be overcome in scientific terms.

[4] Another notable fact that has been established to date is that the shear rupture process is governed by the constitutive law. However, a question arises as to how scale-dependent physical quantities inherent in the shear rupture of a broad scale range from 10^{-3} to 10^{5} m can be treated unifyingly and quantitatively in terms of a single constitutive law. In other words, can the constitutive law that governs the shear rupture process be formulated so as to scale scale-dependent physical quantities inherent in the rupture consistently? If this is possible, a unified comprehension will be provided for scale-dependent physical quantities inherent in the rupture of any size scale, and

[1]Also at Department of Earth Sciences, University College London, London, UK.

0148-0227/03/2000JB000123$09.00

the above mentioned "fracture energy paradox" may be overcome.

[5] It has been established that the earthquake source at shallow crustal depths is a shear rupture instability that takes place on a preexisting fault characterized by inhomogeneities. In fact, there are increasing amounts of commanding evidence that an earthquake fault is inherently inhomogeneous [e.g., *Aki*, 1979, 1984; *Kanamori*, 1981; *Kanamori and Stewart*, 1978; *Bouchon*, 1997]. An inhomogeneous fault includes local, strong patches of high resistance to rupture growth. If a preexisting fault is very weak everywhere on the entire fault, an adequate amount of the elastic strain energy as a driving force to bring about a large earthquake cannot be stored in the medium surrounding the fault. For the adequate amount of the elastic strain energy to be stored in the surrounding medium, strong patches of high resistance to rupture growth are needed on the fault. Such strong patches are also needed for generating strong motion seismic waves.

[6] High resistance to rupture growth may be attained at portions of fault bend or stepover, at interlocking asperities on the fault surfaces, and/or at portions of cohesion healed between the mating surfaces during the interseismic period. These portions (or patches) of high resistance to rupture growth on a fault may be a physical manifestation of what is called "barrier" [*Aki*, 1979, 1984] or "asperity" [*Kanamori and Stewart*, 1978; *Kanamori*, 1981]. Noting that the upper end-member of the strength of such patches is the shear fracture strength of intact rock in seismogenic environments at crustal depths [e.g., *Ohnaka*, 1996; *Ohnaka et al.*, 1997], it follows that the earthquake rupture is not a simple process of frictional slip failure, but a mixed process between what is called frictional slip failure and the shear fracture of initially intact rock. If, therefore, there is any constitutive law that governs the earthquake rupture, the law should be formulated as a unifying constitutive law that governs both frictional slip failure and shear fracture of intact rock.

[7] In this paper, we will first explore how a single constitutive law can unify laboratory data on both frictional slip failure and shear fracture of intact rock. We will then derive a constitutive scaling law that provides a unified comprehension for small-scale shear fracture and frictional slip failure in the laboratory. It will be shown from this scaling law that the constitutive law itself has an inherent property of scale dependence; otherwise, scale-dependent physical quantities inherent in the rupture over a vast scale range cannot be scaled consistently and quantitatively in terms of a single constitutive law. Finally, we wish to show on the basis of the laboratory-based constitutive scaling law that a unified comprehension can be provided for scale-dependent physical quantities inherent in the shear rupture over a broad range from laboratory-scale to field-scale, including large earthquake sources.

2. Constitutive Formulation

[8] Two different approaches have been used to formulate the constitutive law for the earthquake rupture: the rate- and state-dependent constitutive formulation [*Dieterich*, 1978, 1979, 1981, 1986; *Ruina*, 1983], and the slip-dependent constitutive formulation [*Ida*, 1972, 1973; *Ohnaka et al.*, 1987, 1997; *Ohnaka and Yamashita*, 1989; *Matsu'ura et al.*, 1992]. In the rate- and state-dependent formulation, the transient response of the shear traction to the slip rate is assumed essentially important, whereas in the slip-dependent formulation, the transient response of the shear traction to the slip displacement is assumed essentially important.

[9] The rate- and state-dependent constitutive formulation developed by *Dieterich* [1978, 1979, 1981, 1986] and *Ruina* [1983] presumes the slip velocity and, at least, one evolving state variable to be independent and fundamental variables, and the shear traction is expressed as a function of these variables. An advantage of this formulation is that it allows one to simulate qualitatively more than one earthquake cycle including the nucleation process. However, the rate- and state-dependent constitutive law is not formulated so as to explain the instability or stability of the shear fracture process of intact material. The rate- and state-dependent law is not a unifying law that governs both shear fracture of intact rock and frictional slip failure on a pre-existing fault. In addition, it has been demonstrated that dynamic rupture process for stick-slip failure and earthquakes does not exhibit the rate- and state-dependence [*Okubo and Dieterich*, 1986; *Beroza and Mikumo*, 1996; *Day et al.*, 1998]. This suggests that the transient response of the shear traction to the slip velocity is of secondary importance.

[10] Alternatively, the slip-dependent constitutive formulation presumes the slip displacement to be an independent and fundamental variable, and the rate- or time dependence to be of secondary importance [see *Ohnaka et al.*, 1997]. In this formulation, the shear traction is expressed as a function of the slip displacement, and the parameters prescribing the law, such as the peak shear strength, the breakdown stress drop, and the breakdown slip displacement are assumed to be an implicit function of the slip velocity or time [*Ohnaka*, 1996; *Ohnaka et al.*, 1997]. As will be demonstrated later, the slip-dependent constitutive law is a unifying law that governs both shear fracture of intact rock and frictional slip failure. In addition, the slip-dependent formulation is also capable of explaining dynamic rupture process quantitatively [e.g., *Ohnaka and Yamashita*, 1989; *Day et al.*, 1998]. We therefore assume a slip-dependent law as the constitutive law for the shear rupture, with parameters that implicitly depend on strain rate or time.

3. Laboratory Data Used for Analysis

3.1. Fracture Data

[11] The shear rupture includes not only frictional slip failure on a plane or thin zone of weakness (or preexisting fault), but also the shear fracture of initially intact materials. As will be discussed in detail later, both shear fracture of intact materials and frictional slip failure can be unified consistently in terms of a single constitutive law. In order to demonstrate that there is a unifying constitutive law that governs both frictional slip failure and shear fracture of intact rock, experimental data sets of both frictional slip failure and shear fracture of intact rock are needed.

[12] Although a large number of laboratory experiments have been conducted to establish the constitutive law for frictional slip failure, few laboratory experiments have been devoted to establishing the constitutive law for the shear fracture of intact rock. Constitutive relations for the shear

Table 1. Laboratory Test Conditions and Constitutive Law Parameters for the Shear Fracture of Intact Tsukuba Granite[a]

No.	P_c, MPa	P_p, MPa	T, °C	θ, deg	τ_p, MPa	$\Delta\tau_b$, MPa	D_c, mm	D_{wc}, mm	G_c, J/m^2
1	197	29	25	30	413.5	152.7	1.96	1.77	7.7×10^4
2	201	140	25	27	287.8	183.2	2.48	2.31	10.5×10^4
3	201	150	25	29	271.8	170.6	2.10	1.94	10.0×10^4
4	201	179	25	19	139.1	102.3	1.28	1.18	4.1×10^4
5	441	49	25	30	382.2	139.2	0.82	0.60	5.7×10^4
6	480	300	25	35	602.9	170.4	1.02	0.82	6.7×10^4
7	480	300	25	32.5	563.9	126.0	0.80	0.54	5.3×10^4
8	480	300	25	30	517.4	54.6	0.55	0.41	1.4×10^4
9	482	297	25	34	468.8	162.3	1.18	0.95	8.3×10^4
10	481	195	25	33	460.0	141.5	1.07	0.86	6.6×10^4
11	481	99	25	30	501.2	87.5	1.02	0.72	4.8×10^4
12	481	30	25	32.6	513.3	179.7	0.92	0.65	7.9×10^4
13	482	11	25	43	770.8	668.4	2.95	2.55	80.0×10^4
14	481	296	103	42	486.9	165.2	1.67	1.42	12.8×10^4
15	482	199	102	30	512.6	115.4	1.14	0.90	5.5×10^4
16	481	100	104	34	556.4	84.6	1.04	0.57	4.2×10^4
17	480	299	200	33	463.5	162.0	1.15	0.93	8.0×10^4
18	480	199	202	35	520.9	95.2	1.07	0.76	4.5×10^4
19	481	100	202	36	539.0	121.6	1.22	1.00	6.9×10^4

[a] P_c, Confining pressure; P_p, pore pressure; T, temperature; θ, fracture angle; τ_p, peak shear strength; $\Delta\tau_b$, breakdown stress drop; D_c, breakdown slip displacement; D_{wc}, slip-weakening displacement; and G_c, fracture energy.

fracture of intact rock can be observed in laboratory experiments if the entire process is controlled by a stiff frame loading system with electronic servo-controls. We have performed systematic laboratory experiments intensively to reveal mechanical constitutive properties for the shear fracture of intact rock in the brittle to brittle-plastic transition regimes under lithospheric conditions. These experiments have been conducted by using a state-of-the-art testing apparatus constructed in the Earthquake Research Institute [*Ohnaka et al.*, 1997], under the scheme of a joint research project on condition that project participants can utilize experimental data for their own research purpose.

[13] From a large number of experimental samples and data on the shear fracture of intact Tsukuba granite, the samples tested in the brittle regime and the corresponding digitized raw records were extracted for the present purpose. The digitized records were sampled at a frequency of 1 Hz with a multichannel analog-to-digital converter with 16-bit resolution. The experimental procedures have been described in an earlier paper [*Ohnaka et al.*, 1997], and the modal analysis of Tsukuba granite has been given elsewhere [*Odedra et al.*, 2001]. It has been demonstrated by the present series of laboratory experiments that the shear fracture of intact granite at temperature of 200°C is purely brittle and identical to that at room temperature [see also *Wong*, 1982b]. Hence, the test results in a temperature range from room temperature to about 200°C were selected for the present study.

[14] Though the data selected for the present study had been analyzed previously [*Ohnaka et al.*, 1997; *Odedra*, 1998], the selected data were completely reanalyzed for the present purpose by the author after the fracture angle was re-measured in the consistent way. The data set reanalyzed is listed in Table 1. These data were obtained under the conditions of confining pressure in the range 197–482 MPa, interstitial pore water pressure in the range 11–300 MPa, and temperature in the range from room temperature to about 200°C at a strain rate of 10^{-5}/s. It has been demonstrated that the effective stress law holds for Tsukuba granite at the strain rate of 10^{-5}/s [*Odedra et al.*, 2001; *Kato et al.*, 2002].

3.2. Frictional Slip Failure Data

[15] To observe constitutive properties of frictional slip failure, a series of high-resolution laboratory experiments have been performed on propagating mode II type shear failure (stick-slip) on preexisting faults, in which the 290 mm long and 50 mm wide mating surfaces act as weak junctions under an applied normal load. The two-axial testing apparatus was used for these experiments at room temperature. The experimental configuration and method have been described in detail in an earlier paper [*Ohnaka and Shen*, 1999]. Tsukuba granite was also selected as test specimens for this series of laboratory experiments on frictional slip failure.

[16] Precut faults with two different surface roughnesses were prepared by lapping the flat surfaces with carborundum grit having different grain sizes, in order to test the effect of the fault surface roughness on the constitutive property of frictional slip failure. The profiles of these fault surfaces were measured with a diamond stylus profilometer with tip radius of 2 μm in the same manner described in the earlier paper [*Ohnaka and Shen*, 1999]. The fault surface roughness that exhibits band-limited self-similarity can be characterized in terms of the following two parameters: (1) the fractal dimension, which is determined from the segment slope of a band, and (2) the characteristic length, which is defined as the corner length that separates the neighboring two bands with different segment slopes [see *Ohnaka and Shen*, 1999]. Of these two parameters, it has been demonstrated that it is the characteristic length λ_c that plays a critical role in scaling scale-dependent physical quantities inherent in the shear rupture [*Ohnaka and Shen*, 1999]. Hence, attention will be paid to λ_c alone in this paper. The characteristic length λ_c for the fault surfaces will be discussed further in next section.

[17] Two sets of data on frictional slip failure were used for the present study. One set of the data was on the

Table 2. Constitutive Law Parameters for Stick-Slip Failure on a Precut Fault Whose Surfaces Have λ_c = 100 μm[a]

No.	τ_p, MPa	$\Delta\tau_b$, MPa	D_c, μm	D_{wc}, μm	G_c, J/m^2
1	1.390	0.023	1.99	1.46	2.3×10^{-2}
2	1.707	0.046	3.00	2.66	6.9×10^{-2}
3	2.293	0.095	4.57	4.25	2.2×10^{-1}
4	1.720	0.111	3.76	3.29	2.1×10^{-1}
5	3.590	0.134	7.44	5.36	5.0×10^{-1}
6	1.403	0.014	1.58	1.17	1.1×10^{-2}
7	1.649	0.024	2.16	1.62	2.6×10^{-2}
8	2.237	0.057	3.90	3.53	1.1×10^{-1}
9	1.740	0.071	3.31	2.75	1.2×10^{-1}
10	3.455	0.091	5.96	4.05	2.7×10^{-1}
11	1.416	0.017	2.53	2.04	2.2×10^{-2}
12	1.647	0.035	2.30	1.94	4.1×10^{-2}
13	2.243	0.066	3.94	3.55	1.3×10^{-1}
14	1.757	0.083	3.20	2.73	1.3×10^{-1}
15	3.355	0.077	4.52	3.09	1.7×10^{-1}
16	1.472	0.028	2.97	2.58	4.1×10^{-2}
17	1.584	0.045	2.85	2.48	6.3×10^{-2}
18	2.243	0.078	3.52	3.19	1.4×10^{-1}
19	1.817	0.093	2.81	2.45	1.3×10^{-1}
20	1.475	0.028	2.84	2.48	3.9×10^{-2}
21	1.578	0.045	2.63	2.26	5.9×10^{-2}
22	2.238	0.063	2.24	1.98	7.1×10^{-2}
23	1.816	0.081	2.08	1.76	8.4×10^{-2}
24	1.474	0.022	2.37	2.11	2.6×10^{-2}
25	1.572	0.039	2.16	1.55	4.2×10^{-2}
26	2.237	0.073	3.31	3.02	1.2×10^{-1}
27	1.818	0.085	2.59	2.25	1.1×10^{-1}

[a] τ_p, Peak shear strength; $\Delta\tau_b$, breakdown stress drop; D_c, breakdown slip displacement; D_{wc}, slip-weakening displacement; and G_c, rupture energy.

nucleation of frictional slip failure that proceeded quasi-statically on a precut fault with rough surface (λ_c = 200 μm), and the other set was on the frictional slip failure that propagated on a precut fault with smoother surface (λ_c = 100 μm). These sets of data were obtained by analyzing unpublished raw data, which had been stored as records digitized either at a sampling frequency of 500 Hz with a multichannel analog-to-digital converter with 14-bit resolution, or at a frequency of 1 MHz with another multichannel analog-to-digital converter with 12-bit resolution [see *Ohnaka and Shen*, 1999]. The analyzed data are summarized in Tables 2 and 3.

4. A Unifying Constitutive Formulation for the Shear Fracture of Intact Rock and Frictional Slip Failure

4.1. Fault Zone and a Characteristic Length Scale

[18] The shear rupture is an inhomogeneous and nonlinear process during which inelastic shear deformation concentrates in a highly localized zone, resulting in bond-shearing and the release of the shear stress along the rupturing surfaces with ongoing slip displacement. The fault zone (or shear zone) may thus be defined as a thin zone in which concentration of shear deformation is highly localized, and in which the macroscopic rupture surfaces are eventually formed. The fault zone may contain asperities on the rupture surfaces, gouge fragments, and/or highly damaged (or high crack density) thin layers consisting of subsidiary, minute cracks developed in the vicinity of the macroscopic rupture surfaces. Note therefore that no matter how thin it may be, actual fault zone formed in a heterogeneous material such as rock necessarily has its own thickness. The effective fault zone thickness may be defined as the thickness of a highly damaged zone characterized by inelastic deformation, and the outside of the fault zone is primarily characterized by elastic deformation.

[19] It should be noted that the shear traction used for the constitutive formulation is neither the shear stress acting on individual asperities, gouge fragments, and/or cracks contained in the fault zone, nor the shear stress acting on the real, macroscopic rupture surfaces eventually formed in the fault zone because these stresses are not observable. The constitutive law for shear rupture needs to be formulated in terms of observable quantities, in such a way that scale-dependent physical quantities inherent in the rupture are scaled consistently in terms of the law. Since the shear stress acting on both walls of the fault zone thickness (see Figure 1) is observable, this has commonly been used as the shear traction for the constitutive formulation [*Ruina*, 1985].

[20] Likewise, the corresponding slip displacement used for the constitutive formulation is the relative displacement between both walls of the fault zone thickness (see Figure 1). The relative displacement between both walls of the fault zone thickness may include integrated amounts of slip associated with individual asperity fractures, growth of subsidiary, minute cracks, and local displacement between contacting gouge fragments in the fault zone. Although an amount of slip associated with an individual asperity fracture, growth of an individual minute crack, or local displacement between contacting gouge fragments in the fault zone is not observable, the overall, relative displacement between both walls of the fault zone thickness is observable. Note therefore that both shear traction and slip displacement used for the constitutive formulation are defined in a macroscopic sense. The relation between the shear traction and the corresponding slip displacement or the slip velocity in the breakdown zone behind a rupture front is particularly important in formulating the constitutive law for the shear rupture.

[21] Actual rupture surfaces of heterogeneous materials are not flat plane, but they inherently exhibit geometric irregularity. It has been demonstrated that the shear rupture process on a preexisting fault is greatly affected by geometric irregularity of the fault surfaces, and that the characteristic length scale representing the geometric irregularity plays a key role in scaling scale-dependent physical quantities inherent in the rupture [*Ohnaka and Shen*, 1999]. It is

Table 3. Constitutive Law Parameters for the Nucleation Process of Stick-Slip Failure on a Precut Fault Whose Surfaces Have λ_c = 200 μm[a]

No.	τ_p, MPa	$\Delta\tau_b$, MPa	D_c, μm	D_{wc}, μm	G_c, J/m^2
1	4.584	0.061	3.10	2.18	9.4×10^{-2}
2	5.512	0.127	8.37	7.39	5.3×10^{-1}
3	2.391	0.046	3.00	2.51	6.9×10^{-2}
4	3.819	0.124	10.73	8.97	6.6×10^{-1}
5	3.190	0.141	13.40	12.59	9.5×10^{-1}
6	2.739	0.173	11.35	10.46	9.8×10^{-1}
7	2.250	0.030	9.00	6.00	1.4×10^{-1}
8	2.081	0.080	18.20	17.77	7.3×10^{-1}

[a] τ_p, Peak shear strength; $\Delta\tau_b$, breakdown stress drop; D_c, breakdown slip displacement; D_{wc}, slip-weakening displacement; and G_c, rupture energy.

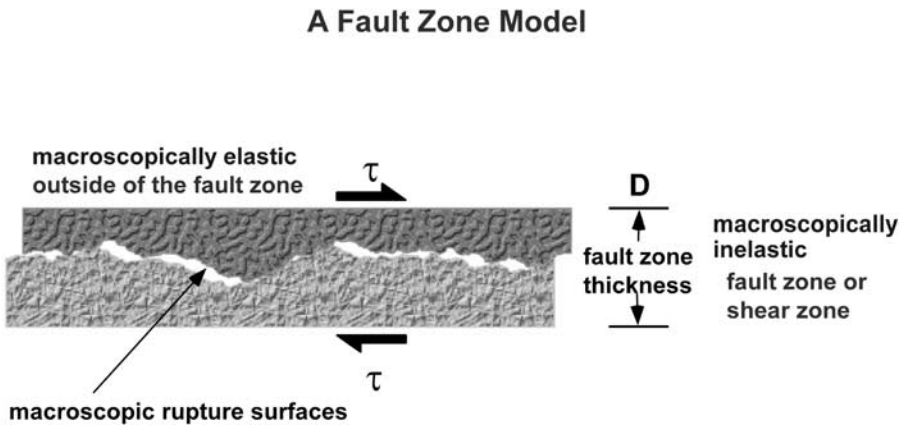

Figure 1. A fault zone model.

therefore necessary to quantify geometric irregularity of shear-fractured surfaces of intact rock in terms of the characteristic length.

[22] There is a persistent idea that rock fracture surfaces exhibit self-similarity at all scales, so that we have investigated to what extent this persistent idea is true. Our elaborate investigation leads to the conclusion that shear-fractured surfaces of intact granite commonly exhibit band-limited self-similarity. This conclusion has reasonable grounds because the slipping process during the breakdown is the process that smoothes away geometric irregularity of the rupturing surfaces. Figure 2a shows an example of the shear-fractured surface profiles for intact granite samples tested. The profiles of these shear-fractured surfaces were measured with a laser-beam profilometer, and the power spectral density was calculated for such topographic profiles. Figure 3 shows a plot of the logarithm of the power spectral density against the logarithm of the wavelength for the profile shown in Figure 2a (curve labeled ''shear fracture surface'').

[23] Since self-similar fracture surfaces are scale-invariant within a finite scale range, the characteristic length λ_c for a shear fracture surface can be defined as the critical wavelength beyond which geometric irregularity of the shear fracture surface no longer exhibits the self-similarity. The characteristic length λ_c defined as such represents a predominant wavelength component of geometric irregularity of the shear-fractured surface. Though both amplitude and wavelength of a predominant component departed from the self-similarity increase with the sample length, they are not only limited by the sample length, but also prescribed by structural heterogeneity of the sample rock fabric, which in turn will be prescribed by spatial distribution of preexisting microcracks and rock-forming mineral grains, their size and shape. When the sample size is fixed, the geometric irregularity and the resulting predominant wavelength component λ_c of shear-fractured surfaces of the intact rock sample will exclusively be prescribed by structural heterogeneity of the rock fabric. From Figure 3, we have $\lambda_c = 6$ mm for this particular fracture surface profile shown in Figure 2a. The characteristic length λ_c of 6 mm is indeed much shorter than the entire length ($\cong$40 mm in this case) and width (16 mm) of the fault formed obliquely across a circular cylinder sample tested.

[24] When a rupture surface has multiple band-limited self-similarities, a different fractal dimension can be calculated for each band, and a characteristic length λ_c can also be defined as the corner wavelength that separates the neighboring two bands with different fractal dimensions. The characteristic length defined as such also represents a predominant wavelength component of geometric irregularity of the rupture surface. The characteristic length defined as the upper fractal limit may be regarded as a special case of this.

[25] Figures 2b and 2c show two examples of the topographic surface profiles of precut faults with two different roughnesses, used for the present experiments on frictional slip failure. The power spectral densities for these fault surface profiles were also calculated, and overplotted in Figure 3 for comparison. From Figure 3, the corner wavelength of 200 μm is found for the rough fault surface shown in Figure 2b, and the corner wavelength of 100 μm is found for the relatively smooth fault surface shown in Figure 2c. These corner wavelengths represent the characteristic length scales for individual fault surfaces, and they are much shorter than the entire fault length (290 mm) and width (50 mm). These characteristic lengths on the precut fault surfaces are primarily prescribed by the surface roughness artificially prepared before the experiments by lapping the flat (ground) surfaces with carborundum grit [*Ohnaka and Shen*, 1999]. Note, therefore, that the amplitude and wavelength of a predominant component of the precut fault surfaces are neither relevant to the sample size nor to the sample rock fabric, but related to grain size of the carborundum grit used.

[26] It will be shown later that the characteristic length scale λ_c defined here plays a key role in not only scaling scale-dependent physical quantities inherent in the rupture, but also unifying laboratory data on the shear fracture of intact rock and frictional slip failure.

4.2. Constitutive Relations Observed for Shear Fracture of Intact Rock

[27] The compressive failure strength of intact rock under confining pressure P_c has conventionally been represented in terms of the differential stress σ_{diff} defined by $\sigma_{diff} = \sigma_1 - \sigma_3$, where σ_1 is the maximum principal stress at failure, and σ_3 is the minimum principal stress, which is equal to P_c.

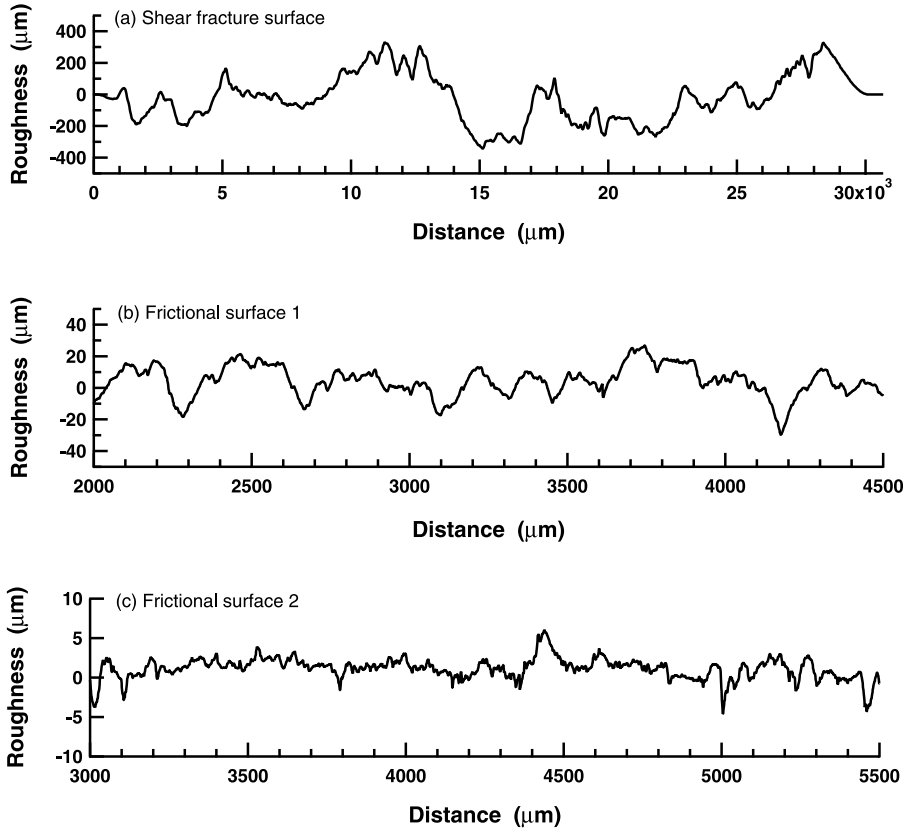

Figure 2. Examples of fault surface profiles. (a) Shear-fracture surface profile of an intact Tsukuba granite sample. (b) Surface profile of a pre-cut fault whose roughness is characterized by the characteristic length λ_c = 200 μm and (c) Surface profile of a pre-cut fault whose roughness is characterized by the characteristic length λ_c = 100 μm.

However, the mechanical failure under combined compressive stress environments commonly occurs by faulting (or shear mode). In order to understand constitutive properties of the shear fracture of intact rock, therefore, it is more appropriate to express the failure strength of intact rock under confining pressure in terms of the resolved shear strength along the macroscopic rupture surfaces, as a function of ongoing slip displacement.

[28] If the fracture angle θ is defined as the angle between the σ_1-axis and the macroscopic fracture plane, the resolved shear stress τ along the macroscopic fracture plane is given by

$$\tau = \frac{1}{2}(\sigma_1 - \sigma_3)\sin 2\theta = \frac{1}{2}(\sigma_1 - P_c)\sin 2\theta, \qquad (1)$$

and the amount of slip displacement D along the fracture plane is given by

$$D = \frac{\Delta l}{\cos\theta} - D_{el}, \qquad (2)$$

where Δl denotes the axial displacement of a test sample, and D_{el} denotes the elastic deformation of the sample. The amount of slip displacement on the rupturing surfaces is defined as the relative displacement between both walls of the rupture zone thickness (see Figure 1).

[29] Figure 4 shows a typical example of the slip-dependent constitutive relation observed for the shear fracture of intact Tsukuba granite. For experimental derivation of a constitutive relation as shown in Figure 4, see an earlier paper [*Ohnaka et al.*, 1997]. It is found from Figure 4 that the shear stress τ initially increases with an increase in the relative displacement D, and that after a peak value τ_p has been attained, τ degrades with ongoing displacement D. The increase in τ with increasing displacement (displacement-hardening) before the peak shear strength is attained is commonly observed for any types of shear failure including frictional slip failure (see Figures 5 and 6).

[30] In the case of compressive loading of initially intact rock, elastic deformation is usually limited to the first 40–50% of the peak strength τ_p (Figure 4). Above this level, micro-cracks develop progressively as the rock is deformed under loading. At higher loads, crack interaction and coalescence become progressively more important, forming a thin, planar zone of higher crack density, which eventually results in the macroscopic shear rupture in the postpeak region where slip-weakening proceeds. Thus, when an intact rock sample in the brittle regime fails in shear mode, nonelastic deformation necessarily concentrates in the zone where the macroscopic shear rupture eventually occurs, and the rate of displacement-hardening decreases as the peak shear strength is approached. The relative displacement D up to the point where the peak strength τ_p is attained consists of integrated amounts of local slip caused by microcracking

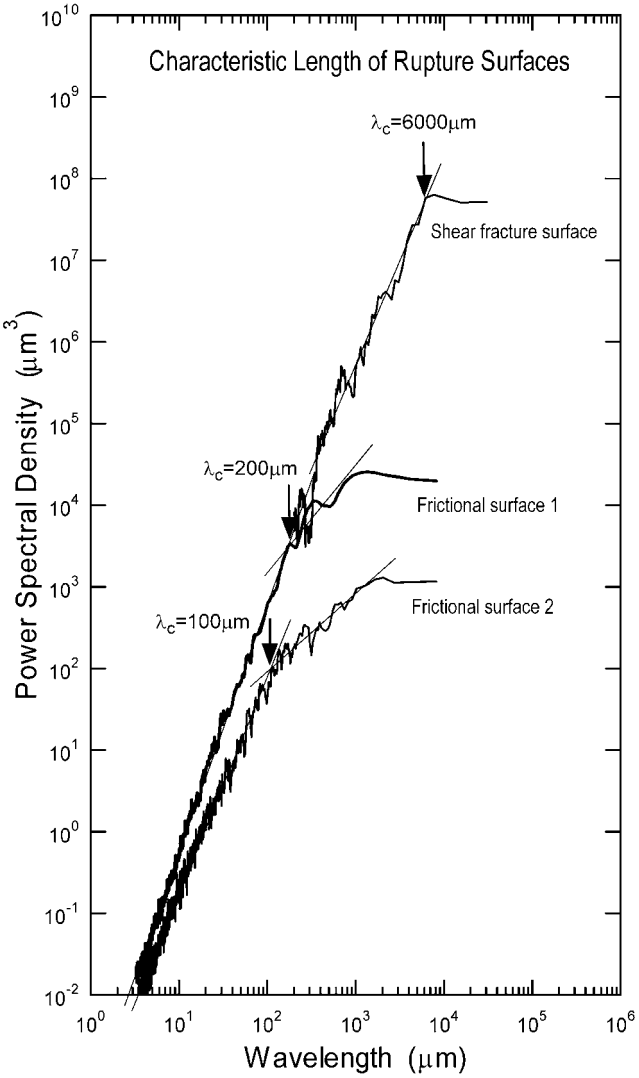

Figure 3. A plot of the logarithm of the power spectral density against the logarithm of the wavelength for a shear fracture surface profile of intact Tsukuba granite shown in Figure 2a, and profiles of pre-cut fault surfaces having different roughnesses shown in Figures 2b and 2c.

that necessarily develops as a preparatory phase of the imminent macroscopic rupture. The preparatory phase of nonelastic deformation during which microcracking, crack-interaction and coalescence develop is therefore an integral part of the eventual macroscopic shear fracture. Without this preparatory phase, intact rock cannot fail macroscopically, so that this phase is a crucial constitutive property for the shear rupture of intact rock, and therefore it must be incorporated into the constitutive relation.

[31] In Figure 4, τ_i denotes the initial stress at which the shear stress τ begins to increase with ongoing displacement D, τ_p denotes the peak shear strength, τ_r denotes the residual friction stress, D_a denotes the critical displacement at which the shear stress has a peak value, D_c denotes the breakdown slip displacement. The breakdown slip displacement D_c is defined as the critical slip displacement required for the shear strength to degrade to τ_r. The breakdown stress drop $\Delta\tau_b$ is defined as $\Delta\tau_b = \tau_p - \tau_r$, and the slip-weakening displacement D_{wc} is defined as the slip displacement required for the shear strength to degrade from τ_p to τ_r. Accordingly,

$$D_{wc} = D_c - D_a, \tag{3}$$

[32] The energy G_c required for the shear rupture is given by [*Palmer and Rice*, 1973]

$$G_c = \int_{D_0}^{D_c} [\tau(D) - \tau_r] dD \tag{4}$$

which equals the area of the shaded portion in Figure 4. In equation (4), $\tau(D)$ represents a constitutive relation between τ and D, and D_0 represents the slip displacement at which the shear stress versus slip displacement curve intersects with the relation $\tau = \tau_r$ (see Figure 4).

[33] The physical quantities τ_i, τ_p, $\Delta\tau_b$, D_a, and D_c specifically prescribe a constitutive relation for the shear rupture, and hence they are crucial parameters for formulating the slip-dependent constitutive law. In particular, the parameters τ_p, $\Delta\tau_b$, and D_c are critically important,

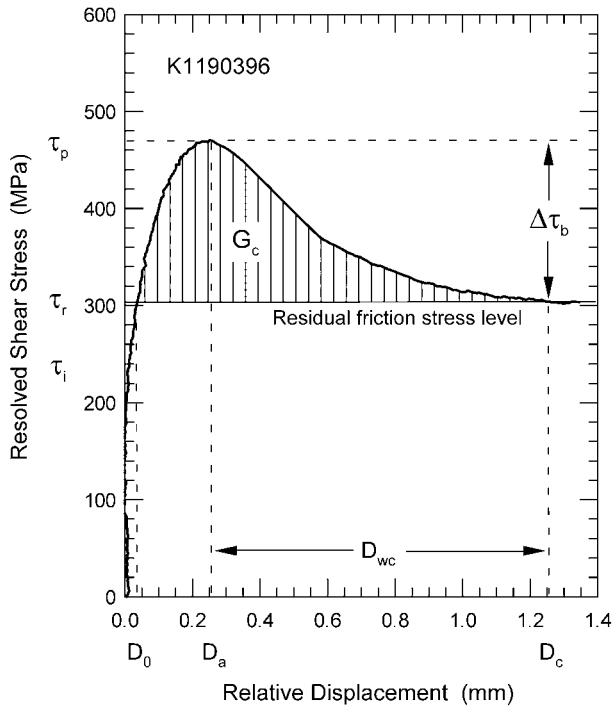

Figure 4. A typical example of the slip-dependent constitutive relation observed for the shear fracture of intact Tsukuba granite. Here τ_i is the critical stress above which the shear stress increases with ongoing displacement, τ_p is the peak shear strength, τ_r is the residual friction stress, $\Delta\tau_b$ is the breakdown stress drop, D_a is the relative displacement required for the shear stress to attain its peak value, D_c is the breakdown slip displacement, D_0 is the displacement at which the shear stress intersects with an extrapolation of the residual friction stress, D_{wc} is the slip-weakening displacement, and G_c is the fracture energy.

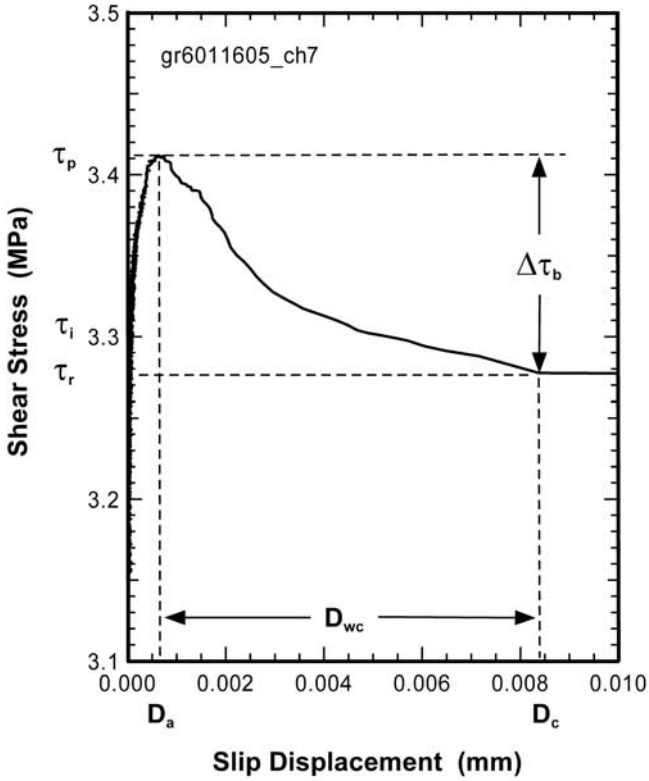

Figure 5. A typical example of the slip-dependent constitutive relation observed near the propagating front of frictional slip failure on a pre-cut fault whose surfaces have the characteristic length λ_c = 100 μm. Here τ_i is the critical stress above which the shear stress increases with ongoing displacement, τ_p is the peak shear strength, τ_r is the residual friction stress, $\Delta\tau_b$ is the breakdown stress drop, D_a is the relative displacement required for the shear stress to attain its peak value, D_c is the breakdown slip displacement, and D_{wc} is the slip-weakening displacement.

because they substantially determine the constitutive property for the shear rupture in a given environment. These constitutive parameters, summarized in Table 1, were evaluated directly from a constitutive relation determined from laboratory experiments at a given ambient test condition.

4.3. Constitutive Relations Observed for Frictional Slip Failure

[34] Figure 5 exemplifies the slip-dependent constitutive relation for frictional slip failure (stick-slip), which was observed near the propagating front of shear rupture on a precut fault whose surfaces have the characteristic length λ_c = 100 μm. The relation between the shear stress and the slip displacement shown in Figure 5 is a constitutive law that governs the instability or stability of frictional slip failure occurring in the breakdown zone behind the propagating rupture front. The breakdown zone is defined as the zone behind the rupture front over which the shear strength degrades transitionally to a residual friction stress level with ongoing slip. The constitutive relation in the breakdown zone is thus characterized by progressive degradation of the shear strength with ongoing slip (Figure 5), which is similar to the constitutive relation observed for the shear fracture of intact rock (Figure 4). The constitutive law parameters τ_p, $\Delta\tau_b$, and D_c (or D_{wc}) for frictional slip failure (stick-slip), summarized in Table 2, have been determined from such a slip-weakening relation as shown in Figure 5.

[35] *Ohnaka and Shen* [1999] have demonstrated with their high-resolution laboratory experiments that the nucleation zone size and its duration of a frictional slip failure event that takes place on a fault having rough surfaces (large λ_c) are much longer than those of the event on a fault having smooth surfaces (small λ_c). This indicates that both size- and time-scales of the nucleation depend on λ_c. With this in mind, data on frictional slip failure events that take place on a fault with rough surfaces (λ_c = 200 μm) were added to the present data set (Table 3). Figure 6 shows an example of the constitutive relation observed during the nucleation of a frictional slip failure event that proceeded quasi-statically on a precut fault with λ_c = 200 μm.

4.4. A Unifying Constitutive Law for Shear Fracture and Frictional Slip Failure

[36] We wish to demonstrate on the basis of laboratory data that the slip-dependent constitutive law is a unifying law that governs both shear fracture of intact rock and frictional slip failure. Figure 7 shows a plot of the logarithm

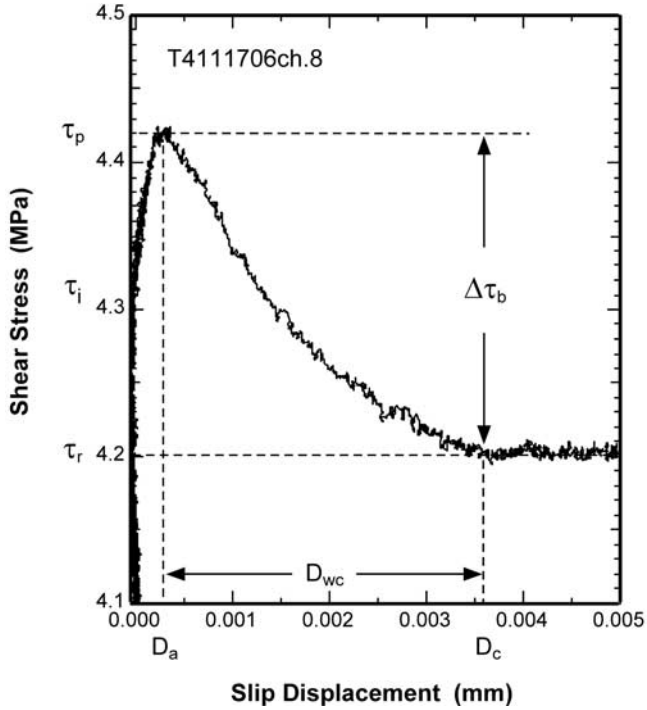

Figure 6. A typical example of the slip-dependent constitutive relation observed during the nucleation of a frictional slip failure event that proceeded slowly on a pre-cut fault whose surfaces have the characteristic length λ_c = 200 μm. Here τ_i is the critical stress above which the shear stress increases with ongoing displacement, τ_p is the peak shear strength, τ_r is the residual friction stress, $\Delta\tau_b$ is the breakdown stress drop, D_a is the relative displacement required for the shear stress to attain its peak value, D_c is the breakdown slip displacement, and D_{wc} is the slip-weakening displacement.

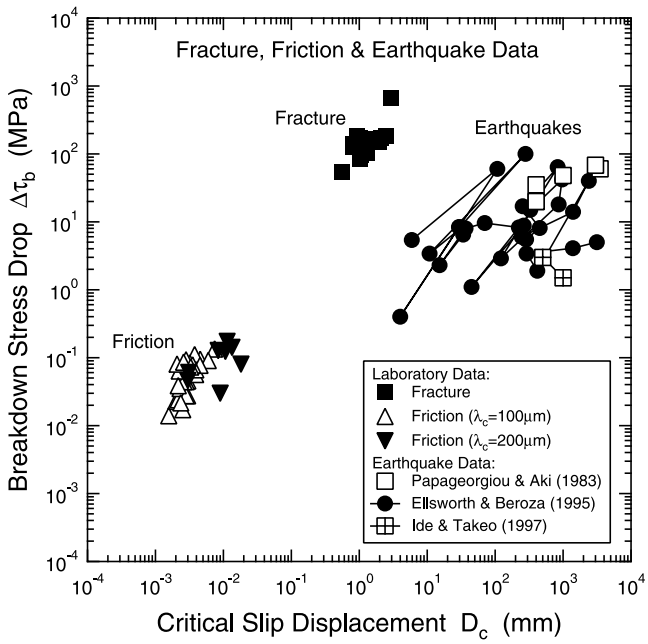

Figure 7. A plot of the logarithm of the breakdown stress drop $\Delta\tau_b$ against the logarithm of the breakdown slip displacement D_c for laboratory data on the shear fracture of intact Tsukuba granite (Table 1) and frictional slip failure on pre-cut faults with two different surface roughnesses (Tables 2 and 3). Field data on earthquake rupture are also overplotted for comparison.

of the breakdown stress drop $\Delta\tau_b$ against the logarithm of the breakdown slip displacement D_c for laboratory data on the shear fracture of intact granite (Table 1), and frictional slip failure on precut faults with two different surface roughnesses (Tables 2 and 3). Black squares in the figure denote data on the shear fracture of intact granite samples, and black and white triangles denote data on the frictional slip failure on precut faults with $\lambda_c = 200$ μm and $\lambda_c = 100$ μm, respectively. The $\Delta\tau_b$ versus D_c relation for earthquakes is also overplotted in Figure 7 for later discussion. We will concentrate on laboratory data alone here, and the comparison between laboratory data on the fracture and frictional slip failure and field data on earthquakes will be made in next section.

[37] It is found from Figure 7 that $\Delta\tau_b$ for the shear fracture of intact granite is the highest among these data sets, while $\Delta\tau_b$ for the frictional slip failure is the lowest. More specifically, $\Delta\tau_b$ is in the range 10^2–10^3 MPa for the shear fracture of intact rock, and in the range 10^{-2} to 2×10^{-1} MPa for frictional slip failure. Thus, $\Delta\tau_b$ for the shear fracture of intact rock is roughly four orders of magnitudes greater than that for frictional slip failure. The large difference in $\Delta\tau_b$ between the shear fracture and the frictional slip failure is partly ascribed to a substantial difference between cohesive strength for intact rock fracture and adhesive strength for frictional slip failure. The difference is also partly ascribed to a difference in the magnitude of normal load (or confining pressure) applied during the experiments on the shear fracture of intact rock and frictional slip failure on a precut fault. To cancel out these effects, $\Delta\tau_b$ needs to be normalized to τ_p, given that τ_p is an increasing function of applied normal load (or confining pressure).

[38] Figure 8 shows a plot of the logarithm of $\Delta\tau_b$ normalized to τ_p against the logarithm of τ_p for the shear fracture data listed in Table 1 and the frictional slip failure data listed in Tables 2 and 3. Black squares in the figure indicate data on the fracture, and black and white triangles indicate data on the frictional slip failure on precut faults with $\lambda_c = 200$ μm and $\lambda_c = 100$ μm, respectively. One can see from this figure that τ_p falls in a range from 100 to 1000 MPa, and $\Delta\tau_b/\tau_p$ in a range from 0.1 to 1 for the shear fracture data. By contrast, τ_p falls in a range from 1 to 10 MPa, and $\Delta\tau_b/\tau_p$ in a range from 0.01 to 0.1 for the frictional slip failure data. It can thus be concluded that the present set of data on the fracture is characterized by high strength and high ratio of the breakdown stress drop to the peak strength, and that the set of data on frictional slip failure is characterized by low strength and low ratio of the breakdown stress drop to the peak strength.

[39] Figure 9 shows a plot of the logarithm of $\Delta\tau_b/\tau_p$ against the logarithm of D_c for the three sets of data on the shear fracture of intact rock (Table 1), and the frictional slip failure (Tables 2 and 3). It is found from Figure 9 that there is a clear positive correlation between $\Delta\tau_b/\tau_p$ and D_c for each set of data on the shear fracture of intact rock, the frictional slip failure on a precut fault with $\lambda_c = 100$ or 200 μm. This indicates that $\Delta\tau_b/\tau_p$ and D_c are interdependent. It is obvious from Figure 9, however, that the entire sets of data on the shear fracture of intact rock and the frictional slip failure are not unified on the $\Delta\tau_b/\Delta\tau_p - D_c$ domain. This is because D_c for the shear fracture of intact rock samples is 2–3 orders of slip amounts greater than D_c for the frictional slip failure. Indeed, D_c for the frictional slip failure in the laboratory ranges from 1 to 20 μm, while D_c

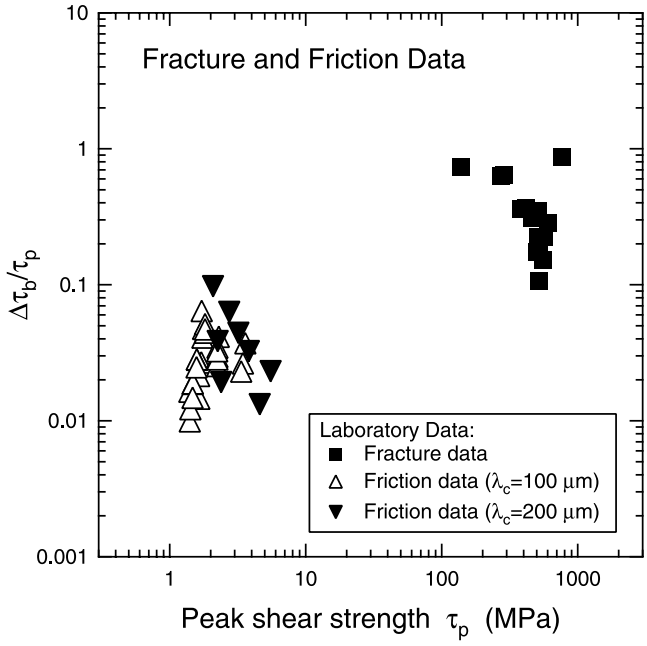

Figure 8. A plot of the logarithm of $\Delta\tau_b$ normalized to τ_p against the logarithm of τ_p for the shear fracture data listed in Table 1, and frictional slip failure data listed in Tables 2 and 3.

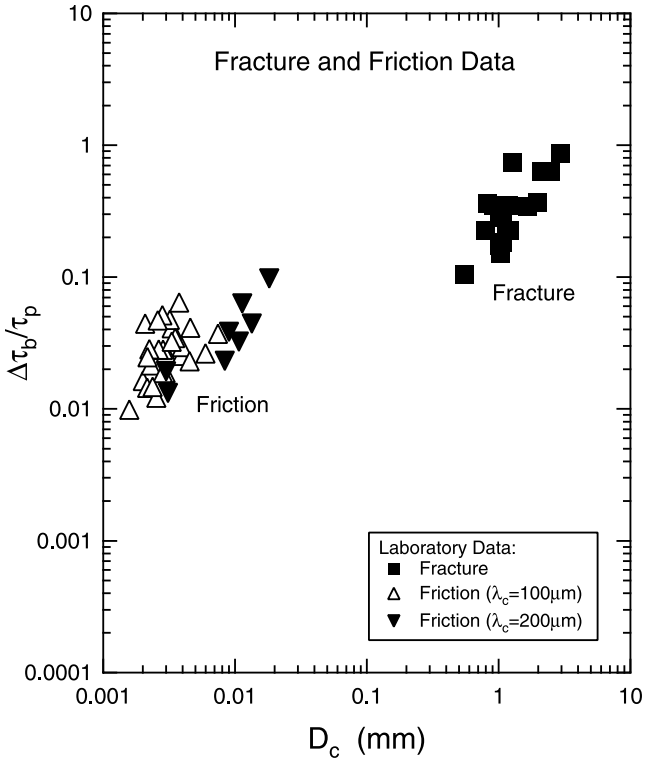

Figure 9. A plot of the logarithm of $\Delta\tau_b/\tau_p$ against the logarithm of D_c for a set of data on the shear fracture of intact Tsukuba granite (Table 1), and two different sets of data on the frictional slip failure (Tables 2 and 3).

for the shear fracture of intact granite samples ranges from 0.5 to 3 mm. In order to provide a unified comprehension for these data sets, D_c on the lateral axis of Figure 9 must be normalized properly.

[40] The breakdown (or slip-weakening) process is severely affected by geometric irregularity of the fault surfaces, and as noted previously, the characteristic length λ_c represents a predominant wavelength component of geometric irregularity of the fault surfaces. It will therefore be natural to expect that D_c scales with λ_c. Figure 10a shows a plot of the logarithm of $\Delta\tau_b/\tau_p$ against the logarithm of D_c/λ_c for the same sets of data on the shear fracture of intact rock (Table 1) and on the frictional slip failure (Tables 2 and 3). Black squares in the figure denote data on the shear fracture, and black and white triangles denote data on the frictional slip failure on precut faults with $\lambda_c = 200$ μm and $\lambda_c = 100$ μm, respectively. It is found from Figure 10a that these different sets of data on the fracture and the frictional slip failure are unified by a single relation on the $\Delta\tau_b/\tau_p - D_c/\lambda_c$ domain. Note also from Figure 10a that the two subsets of data on the frictional slip failure listed in Table 2 ($\lambda_c = 100$ μm) and Table 3 ($\lambda_c = 200$ μm) are also unified within experimental errors.

[41] We find from Figure 10a that the relation between $\Delta\tau_b/\tau_p$ and D_c/λ_c is well represented by a power law of the form

$$\frac{\Delta\tau_b}{\tau_p} = \beta\left(\frac{D_c}{\lambda_c}\right)^M, \tag{5}$$

where β and M are numerical constants. The double-error regression analysis [*York*, 1966] of the entire data sets plotted in Figure 10a leads to the following values for β and M with their standard deviations: $\beta = 1.64 \pm 0.29$ and $M = 1.20 \pm 0.06$. The correlation coefficient for these data points is 0.933. In this analysis, equal weights of the values for both $\Delta\tau_b/\tau_p$ and D_c/λ_c have been assumed. Relation (5) represents a constraint to be imposed on the constitutive parameters τ_p, $\Delta\tau_b$, and D_c. *Ohnaka* [1992, 1996] has suggested a similar relation of power law of the form

$$\Delta\tau_b = \Delta\tau_{b0}\left(\frac{D_c}{\lambda_c}\right)^M \tag{6}$$

for frictional slip failure (stick-slip), where $\Delta\tau_{b0}$ and M (=1.2) are constants. This relation can be included in more general expression (5) by assuming that $\Delta\tau_{b0} = \beta\tau_p$.

[42] The breakdown slip displacement D_c is the sum of the displacement D_a required for the shear stress to increase up to the peak strength τ_p, and the displacement D_{wc} required for the shear strength to degrade from τ_p to a residual friction stress level τ_r. By definition, D_a is the critical displacement responsible for the displacement-hardening (or strengthening), and D_{wc} is the critical displacement responsible for the slip-weakening. One may therefore expect that the relation between $\Delta\tau_b/\tau_p$ and D_{wc}/λ_c will also be represented by a power law of the form similar to equation (5). This has been checked. Figure 10b shows a plot of the logarithm of $\Delta\tau_b/\tau_p$ against the logarithm of D_{wc}/λ_c for the fracture data (Table 1) and the frictional slip failure data (Tables 2 and 3). We find from Figure 10b that the relation between $\Delta\tau_b/\tau_p$ and D_{wc}/λ_c obeys a power law of the form

$$\frac{\Delta\tau_b}{\tau_p} = \beta'\left(\frac{D_{wc}}{\lambda_c}\right)^M, \tag{7}$$

where β' and M are numerical constants. The double-error regression analysis for these data points gives the following values for β' and M with their standard deviations: $\beta' = 2.26 \pm 0.38$ and $M = 1.20 \pm 0.055$, and 0.954 for the correlation coefficient.

[43] Relation (7) is equivalent with relation (5). The present laboratory data showed that the exponent of (D_{wc}/λ_c) in equation (7) coincides with the exponent of (D_c/λ_c) in equation (5). This leads to the conclusion that both D_{wc} and D_a are directly proportional to D_c. We indeed have from equations (5) and (7) that

$$D_{wc} = \left(\frac{\beta}{\beta'}\right)^{1/M} D_c = 0.766 D_c \tag{8}$$

and from equations (3) and (8), we have

$$D_a = \left[1 - \left(\frac{\beta}{\beta'}\right)^{1/M}\right] D_c = 0.234 D_c \tag{9}$$

[44] The proportional relationships (8) and (9) can be confirmed directly from the present sets of data on D_{wc} and D_c for the shear fracture (Table 1) and the frictional slip

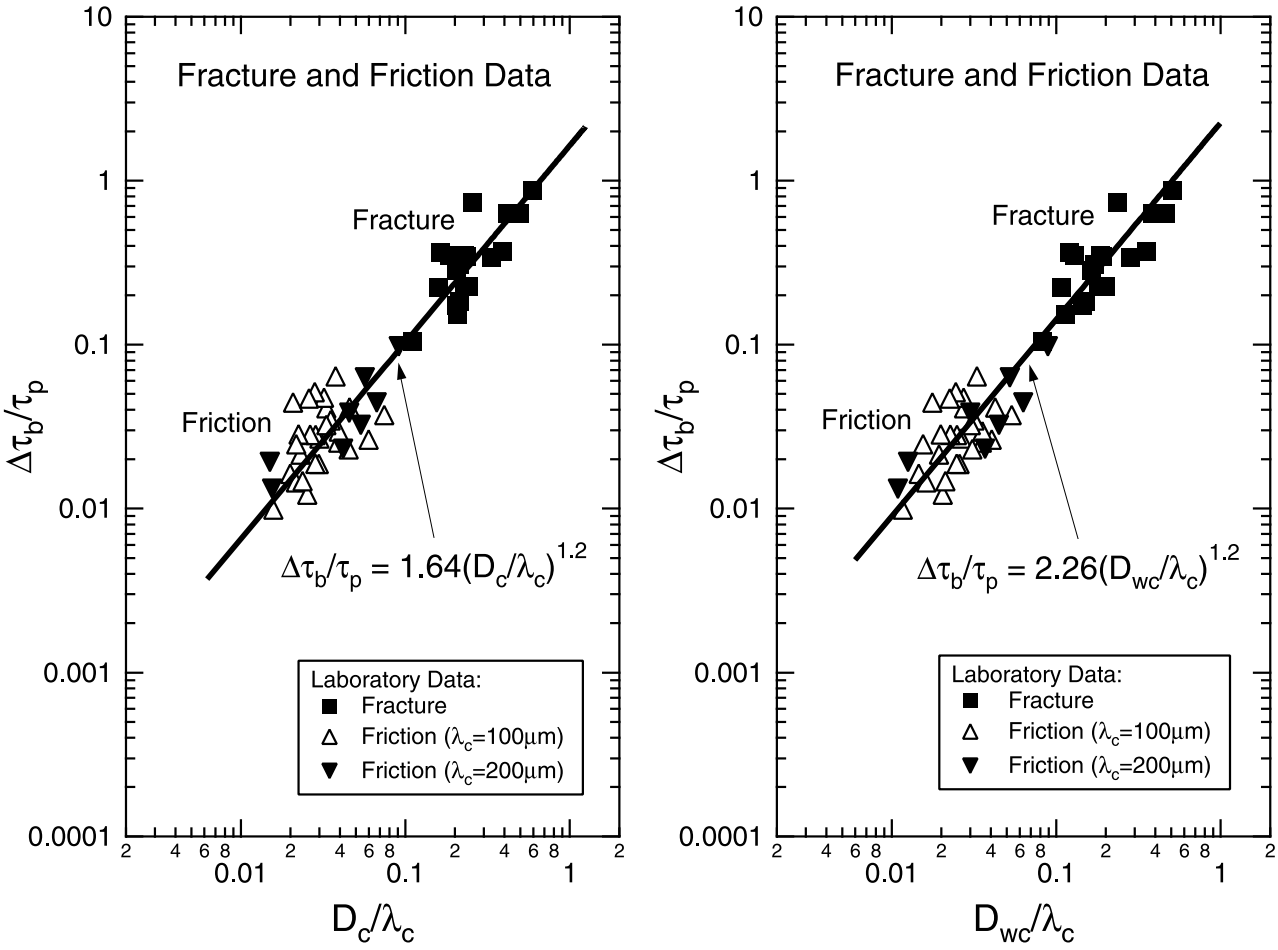

Figure 10. A plot of (a) the logarithm of $\Delta\tau_b/\tau_p$ against the logarithm of D_c/λ_c, and (b) the logarithm of $\Delta\tau_b/\tau_p$ against the logarithm of D_{wc}/λ_c, for three different sets of data on the shear fracture (Table 1) and the frictional slip failure (Tables 2 and 3).

failure (Tables 2 and 3). Figure 11a shows a plot of D_{wc} against D_c for the sets of data on the shear fracture and the frictional slip failure, and Figure 11b shows a plot of D_a against D_c for the same data sets. One can see from Figure 11 that the plot of D_{wc} against D_c is well represented by relation (8), and that the plot of D_a against D_c is represented by relation (9). Figure 11 also shows that both fracture and frictional slip failure data are consistently unified by a single constitutive law.

[45] The direct proportional relationship between D_c and D_{wc} indicates that the parameters D_c and D_{wc} are mutually equivalent, as noted above. In addition, the proportional relationships (8) and (9) show that the critical weakening displacement D_{wc} is predictable from the critical hardening displacement D_a. This implies that the preceding process of displacement-hardening can substantially prescribe the displacement-weakening process. This suggests that the constitutive parameters D_a, D_{wc}, and D_c may be described in terms of the common, underlying physics.

[46] It has been found that laboratory data on both shear fracture of intact rock and frictional slip failure are unified consistently by a single relation (5), or equivalent relation (7). It has also been found that constitutive law parameters such as τ_p, $\Delta\tau_b$, D_a, and D_c are interdependent, and that they are mutually constrained by several relations (3), (5), and (7)–(9). Of these relations, only three equations are independent. Hence, equations (3), (5), and (8) will be regarded as independent hereafter, and the following three constitutive parameters: τ_p, $\Delta\tau_b$, and D_c will be regarded as fundamental.

4.5. A Constitutive Scaling Law

[47] The slip-dependent constitutive law for the shear rupture is specifically prescribed by the following five parameters: τ_i, τ_p, $\Delta\tau_b$, D_a, and D_c (or D_{wc}). Of these, the displacement parameters D_a, and D_c (or D_{wc}) are scale-dependent. Rewriting relation (5), we have

$$D_c = m(\Delta\tau_b/\tau_p)\lambda_c \tag{10}$$

where $m(\Delta\tau_b/\tau_p)$ is a dimensionless parameter which is a function of $\Delta\tau_b/\tau_p$. The dimensionless parameter m is written as

$$m(\Delta\tau_b/\tau_p) = \left(\frac{1}{\beta}\right)^{1/M}\left(\frac{\Delta\tau_b}{\tau_p}\right)^{1/M} = 0.662\left(\frac{\Delta\tau_b}{\tau_p}\right)^{0.833} \tag{11}$$

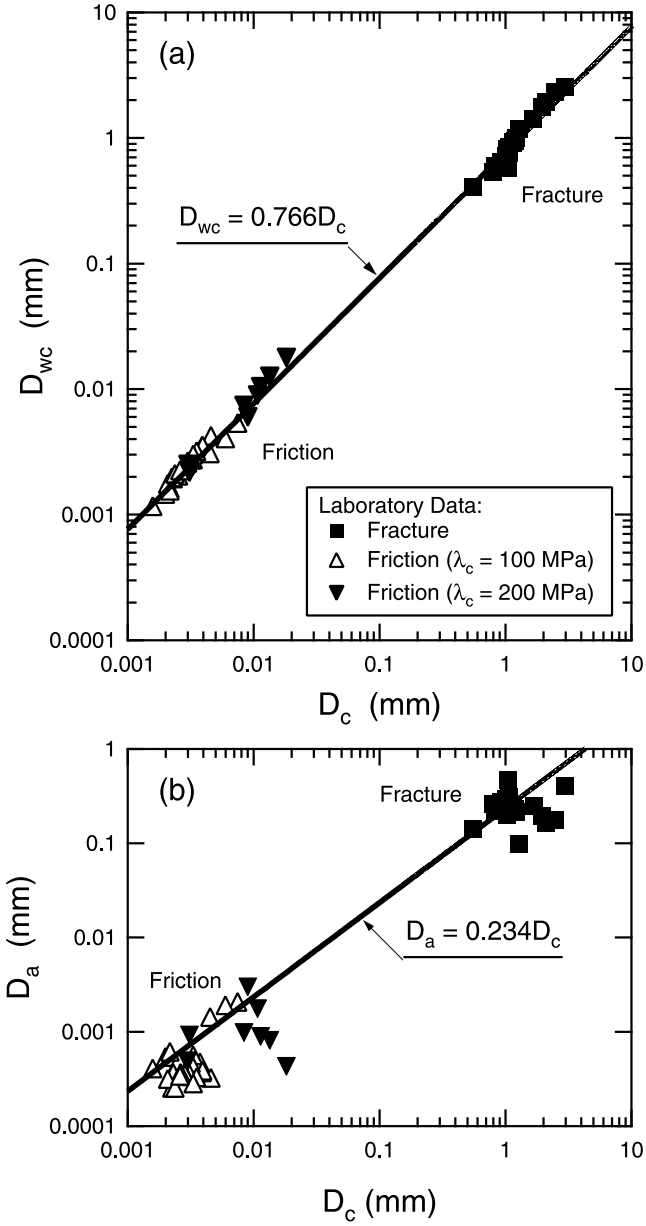

Figure 11. A plot of (a) the logarithm of D_{wc} against the logarithm of D_c, and (b) the logarithm of D_a against the logarithm of D_c, for three different sets of data on the shear fracture (Table 1) and the frictional slip failure (Tables 2 and 3).

From (8), (9), and (10), we have

$$D_{wc} = \left(\frac{\beta}{\beta'}\right)^{1/M} m(\Delta\tau_b/\tau_p)\lambda_c = 0.766 \times m(\Delta\tau_b/\tau_p)\lambda_c \quad (12)$$

and

$$D_a = \left[1 - \left(\frac{\beta}{\beta'}\right)^{1/M}\right] m(\Delta\tau_b/\tau_p)\lambda_c = 0.234 \times m(\Delta\tau_b/\tau_p)\lambda_c \quad (13)$$

[48] It is confirmed from relations (10), (12), and (13) that all the displacement parameters D_c, D_{wc}, and D_a scale with λ_c, since $\Delta\tau_b/\tau_p$ is scale-independent. In particular, they are directly proportional to λ_c if $\Delta\tau_b/\tau_p$ is constant. Yet, the proportional relationship between λ_c and either D_c, D_{wc} or D_a is violated by the fluctuation of $\Delta\tau_b/\tau_p$, because $\Delta\tau_b/\tau_p$ in general can take different values according to the test conditions. In this sense, a specific scaling relation between D_c (or D_{wc} or D_a) and λ_c depends entirely on $\Delta\tau_b/\tau_p$. Figure 12 shows how the parameter m (= D_c/λ_c) depends on $\Delta\tau_b/\tau_p$. The parameter m is a monotonically increasing function of $\Delta\tau_b/\tau_p$, and it has the maximum value of 0.66 at $\Delta\tau_b/\tau_p = 1$. For data on the shear fracture of intact granite listed in Table 1, $\Delta\tau_b/\tau_p$ has a value ranging from 0.1 to 1 (see Figure 8 or 9), and in this case, m takes a value ranging from 0.1 to 0.66. By contrast, for data on the frictional slip failure listed in Tables 2 and 3, $\Delta\tau_b/\tau_p$ has a value ranging from 0.01 to 0.1 (Figure 8 or 9), and in this case, m takes a value ranging from 0.015 to 0.1.

[49] It has been demonstrated that the displacement-related constitutive parameters D_c, D_{wc}, and D_a scale specifically with λ_c. The characteristic length λ_c has been defined as the critical wavelength departed from the self-similarity for geometric irregularity of the rupture surfaces. Therefore, scaling of D_c, D_{wc}, and D_a is directly related to geometric property of the macroscopic rupture surfaces. It has been shown that scaling of scale-dependent physical quantities inherent in the rupture is theoretically ascribed to the scale-dependence of D_c [*Ohnaka and Shen*, 1999; *Ohnaka*, 2000].

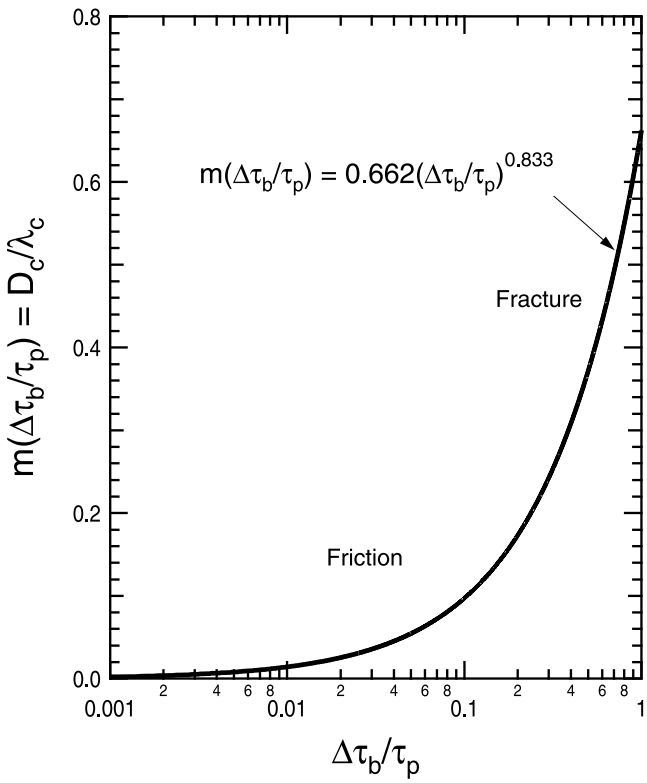

Figure 12. A plot of the non-dimensional parameter m against $\Delta\tau_b/\tau_p$. Note that $\Delta\tau_b/\tau_p$ falls in a range from 0.1 to 1 for the shear fracture data listed in Table 1, and in a range from 0.01 to 0.1 for the frictional slip failure data listed in Tables 2 and 3 (see Figure 8 or 9).

It thus follows that constitutive scaling law (10) plays a fundamental role in not only unifying laboratory data on the shear fracture of intact rock and frictional slip failure, but also scaling scale-dependent physical quantities inherent in the rupture. This will be further discussed below.

4.6. Apparent Shear Rupture Energy

[50] When a constitutive relation $\tau(D)$ is specifically given, the shear rupture energy G_c can be evaluated directly by integrating equation (4). Indeed, G_c listed in Table 1 for the shear fracture of intact granite samples tested in the laboratory was directly calculated from equation (4). On the other hand, G_c is expressed explicitly in terms of the constitutive law parameters $\Delta\tau_b$ and D_c [*Ohnaka and Yamashita*, 1989] by

$$G_c = \frac{\Gamma}{2}\Delta\tau_b D_c \tag{14}$$

where Γ is a dimensionless parameter defined by

$$\Gamma = \int_0^1 \frac{\sigma(Y)}{\sqrt{Y}}dY \tag{15}$$

where $\sigma(Y)$ is the nondimensional shear strength at a nondimensional distance Y measured from the rupture front in the breakdown zone.

[51] Equation (14) allows one to estimate G_c from the constitutive law parameters $\Delta\tau_b$ and D_c, if Γ is known. If a simplified, linear slip-weakening relation is assumed, Γ is exactly unity. However, laboratory-based slip-dependent constitutive relations are found to be nonlinear (see Figures 4–6). Even if non-linear constitutive relations observed in the laboratory are considered, it is evaluated that Γ has a value ranging from 1/2 to unity [*Ohnaka and Yamashita*, 1989; *Ohnaka et al.*, 1997]. It may thus be concluded that Γ = 1/2 to 1.

[52] The shear rupture energy G_c defined by equation (4) may be rewritten as

$$G_c = G_{c1} + G_{c2} \tag{16}$$

where

$$G_{c1} = \int_{D_0}^{D_a} [\tau(D) - \tau_r]dD \tag{17}$$

and

$$G_{c2} = \int_{D_a}^{D_c} [\tau(D) - \tau_r]dD \tag{18}$$

G_{c1} represents the fracture energy integrated for numerous microcrackings that develop before the macroscopic shear fault is formed, and G_{c2} represents the energy required for the breakdown from the peak strength to a residual friction stress during the macroscopic shear faulting [*Ohnaka et al.*, 1997]. The definition of the shear fracture energy by equation (18) has been employed by *Rice* [1980] and *Wong* [1982a, 1986]. As noted earlier, however, the phase of nonelastic deformation during which microcracking develops before the macroscopic shear faulting occurs, is an integral part of the eventual, macroscopic shear rupture. Without this phase, intact rock cannot fail macroscopically. In other words, it is not only G_{c2} but also G_{c1} that is needed for rupturing an intact material, and hence G_{c1} cannot be neglected. For this reason, the rupture energy defined by equations (4) or (16) is used in this paper.

[53] We wish to demonstrate that the two sets of laboratory data on G_c for the shear fracture of intact rock (Table 1) and the frictional slip failure (Tables 2 and 3) can be unified, if a slip-dependent constitutive law on which the constraint (10) is imposed is assumed as the governing law for the shear rupture. Combining equations (10) and (11) with equation (14) leads to the following expression for G_c

$$G_c = \frac{\Gamma}{2}\left(\frac{1}{\beta}\right)^{1/M}\Delta\tau_b\left(\frac{\Delta\tau_b}{\tau_p}\right)^{1/M}\lambda_c \tag{19}$$

Equation (19) predicts that G_c should directly scale with λ_c, showing that G_c is scale-dependent.

[54] Why G_c is scale-dependent may be understood from the fact that real rupture surfaces of inhomogeneous materials such as rock cannot be flat plane, but they necessarily exhibit geometric irregularity (or roughness). If the rupture surfaces are flat plane, G_c cannot be scale-dependent. However, the real area of geometrically irregular rupture surface is significantly different from the apparent area of "rupture plane". The rougher the ruptured surfaces, the larger the real surface area becomes, and λ_c becomes longer for rougher surfaces having band-limited fractal nature. For this reason, G_c is not only dependent on the material property, but also scale-dependent. This fact is overlooked when G_c is evaluated. G_c defined by equation (4) or (14) may thus be called the apparent rupture (or fracture) energy.

[55] Equation (19) can be rewritten as:

$$\frac{G_c}{\tau_p\lambda_c} = \frac{\Gamma}{2}\left(\frac{1}{\beta}\right)^{1/M}\left(\frac{\Delta\tau_b}{\tau_p}\right)^{(M+1)/M} \tag{20}$$

or equivalently

$$\frac{G_c}{\tau_p\lambda_c} = \frac{\Gamma\beta}{2}\left(\frac{D_c}{\lambda_c}\right)^{M+1} \tag{21}$$

Relations (20) and (21) predict that if $G_c/(\tau_p\lambda_c)$ is plotted against $\Delta\tau_b/\tau_p$ or D_c/λ_c, a unified comprehension should be provided for the energy for both shear fracture of intact rock and frictional slip failure. Figure 13a shows a plot of the logarithm of $G_c/(\tau_p\lambda_c)$ against the logarithm of $\Delta\tau_b/\tau_p$ for the shear fracture data listed in Table 1, and the frictional slip failure data listed in Tables 2 and 3. Figure 13b shows a plot of the logarithm of $G_c/(\tau_p\lambda_c)$ against the logarithm of D_c/λ_c for the same data sets. Black squares in Figure 13 indicate data on the fracture of intact granite, black triangles indicate data on frictional slip failure on a precut fault with the rough surface (λ_c = 200 μm), and white triangles indicate frictional slip failure on a precut fault with the smoother surface (λ_c = 100 μm).

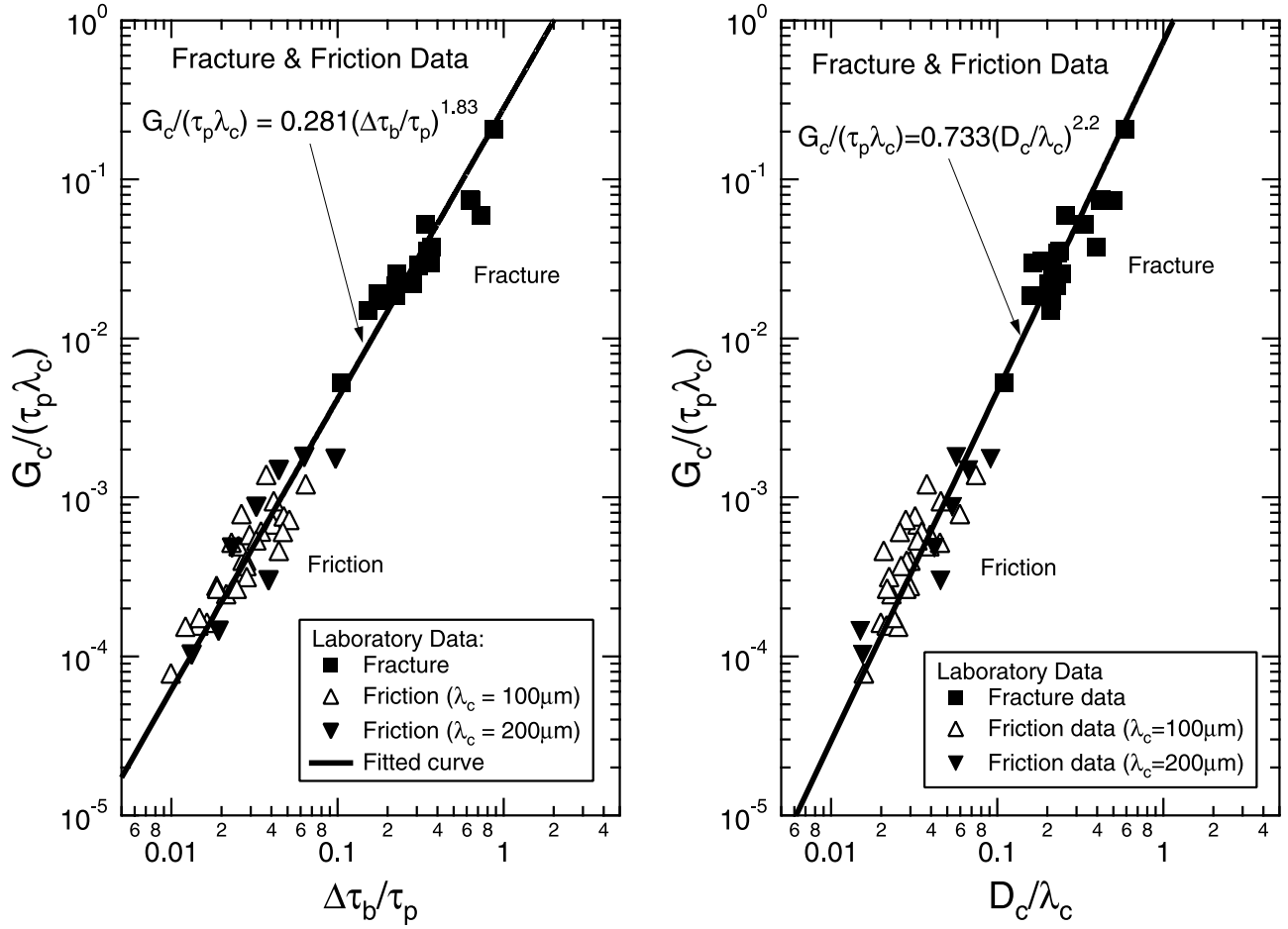

Figure 13. A plot of (a) the logarithm of $G_c/(\tau_p\lambda_c)$ against the logarithm of $\Delta\tau_b/\tau_p$, and (b) the logarithm of $G_c/(\tau_p\lambda_c)$ against the logarithm of D_c/λ_c, for three different sets of data on the shear fracture (Table 1) and the frictional slip failure (Tables 2 and 3).

[56] It is found from Figure 13 that the shear fracture energy of intact rock samples and the shear failure energy of frictional slip are unified by a single law of the form (20) or (21). When the exponent of $(\Delta\tau_b/\tau_p)$ is fixed to be 1.83 (= $(M + 1)/M$), the double-error regression analysis of these data points gives

$$\frac{G_c}{\tau_p\lambda_c} = (0.281 \pm 0.038)\left(\frac{\Delta\tau_b}{\tau_p}\right)^{1.83}, \quad r = 0.984 \qquad (22)$$

where r is the correlation coefficient. From (20) and (22), $(\Gamma/2)(1/\beta)^{1/M} = 0.281$, and the substitution of 1.64 for β and 1.20 for M leads to $\Gamma = 0.85$. Likewise, when the exponent of D_c/λ_c is fixed to be 2.2 (=M + 1), the regression analysis for the same data sets gives

$$\frac{G_c}{\tau_p\lambda_c} = (0.733 \pm 0.182)\left(\frac{D_c}{\lambda_c}\right)^{2.2}, \quad r = 0.961 \qquad (23)$$

From equations (21) and (23), $\Gamma\beta/2 = 0.733$, and the substitution of 1.64 for β leads to $\Gamma = 0.89$. The common result that $\Gamma = 0.85 \sim 0.89$ is very reasonable, noting that these values for Γ fall in between 0.5 and 1.

[57] In Figure 13, G_c has been normalized to the product of τ_p and λ_c. Nevertheless, it is found from Figure 13 that the normalized G_c is an increasing function of $\Delta\tau_b/\tau_p$ or D_c/λ_c. In addition, the normalized G_c for the shear fracture of intact rock is greater than that for frictional slip failure. This is a manifestation of the fact that cohesive bond strength for intact rock fracture is the upper end-member of adhesive strength for frictional slip failure.

5. Scaling of Scale-Dependent Physical Quantities and a Unification of Laboratory Data With Earthquake Data

[58] We examine specifically how scale-dependent physical quantities inherent in the rupture are scaled, and how laboratory data on both shear fracture of intact rock and frictional slip failure can be unified with field data on earthquake rupture, under the assumptions that a laboratory-based slip-dependent constitutive law is the governing law for the earthquake rupture, and that the governing law is constrained by relation (5), or constitutive scaling law (10), with $\beta = 1.64$ and $M = 1.20$.

5.1. Breakdown Slip Displacement

[59] One of the crucial results in the previous sections is that D_c is scale-dependent. This is corroborated from the data shown in Figure 7. In Figure 7, white squares are

earthquake data taken from *Papageorgiou and Aki* [1983], black circles from *Ellsworth and Beroza* [1995], and white squares with cross from *Ide and Takeo* [1997]. These earthquake data have been compiled in Table 1 in an earlier paper [*Ohnaka*, 2000]. Since *Ellsworth and Beroza* [1995] did not evaluate D_c for earthquakes in their paper, the author [*Ohnaka*, 2000] has evaluated D_c for these earthquakes, and the evaluated values of D_c have also been listed in Table 1 in the earlier paper.

[60] We find from Figure 7 that $\Delta\tau_b$ for earthquakes is in a range from 1 to 100 MPa, and falls in between $\Delta\tau_b$ for the shear fracture of intact rock and that for frictional slip failure in the laboratory. Since $\Delta\tau_b$ for earthquakes is not allowed to exceed the magnitude of $\Delta\tau_b$ for the shear fracture of intact rock at seismogenic crustal conditions, $\Delta\tau_b$ for earthquakes is of the same order (or less) of magnitude of $\Delta\tau_b$ for the shear fracture tested in the laboratory. In other words, $\Delta\tau_b$ for the shear fracture of intact rock is the upper end-member of $\Delta\tau_b$ for earthquake rupture (see also Figure 16). Recent laboratory experiments suggest that $\Delta\tau_b$ slightly decreases with a decrease in strain rate [*Kato et al.*, 2001]. If this is the case, the strain rate effect will also contribute to a smaller value of $\Delta\tau_b$ for earthquakes than that for the shear fracture of intact rock tested in the laboratory, since tectonic strain rates are much slower than the strain rate of 10^{-5}/s in the laboratory.

[61] We also find from Figure 7 that earthquake data points do not fall on the trend of either the fracture data or the friction data. They deviate systematically from both trends, showing that the amount of D_c for earthquakes is much larger than that of D_c for the shear fracture and frictional slip failure in the laboratory. In particular, we find that D_c for major earthquakes is in a range from a few tens of centimeters to several meters. This is contrasted with the amount of D_c observed in the laboratory, which is in a range from 0.5 to 3 mm for the shear fracture of intact rock samples, and in a range from 1 to 20 μm for frictional slip failure on a precut fault with λ_c = 100 or 200 μm. Recent laboratory experiments indicate that D_c tends to decrease with a decrease in strain rate [*Kato et al.*, 2001]. Nevertheless, D_c for large-scale earthquake rupture (caused at a slow tectonic strain rate) is much larger than D_c for small-scale rupture (caused at a laboratory strain rate of 10^{-5}/s) (see Figure 7). This shows that the systematic difference in the amount of D_c between laboratory and field data is ascribed to the scale-dependence of D_c, and that the effect of strain rate on D_c is negligibly small compared with the scale-dependence of D_c.

[62] The scale-dependence of D_c has been derived from laboratory data alone in previous section, and this scale-dependence is further corroborated by the comparison between field- and laboratory-scale rupture data in Figure 7. It is thus obvious that D_c for large-scale earthquake rupture is much larger than that for small-scale rupture in the laboratory. This is contrasted with another fact that $\Delta\tau_b$ for large-scale earthquake rupture is of the same order of magnitude (or less) of that for small-scale fracture in the laboratory, indicating that $\Delta\tau_b$ is scale-independent [*Ohnaka*, 2000]. Seismological analyses show that amounts of D_c for large earthquakes are as large as on the the order of 1 m (see Figure 7). However, there is a persistent hypothesis that D_c for large earthquakes is as small as the amount of D_c for small-scale shear rupture observed in the laboratory. We therefore discuss below how the present result is justified and corroborated from other independent data.

[63] The peak slip velocity $\dot{D}_{\max}$ and the peak slip acceleration $\ddot{D}_{\max}$ on a dynamically propagating fault are expressed in terms of the slip-dependent constitutive law parameters $\Delta\tau_b$ and D_c as [*Ida*, 1973; *Ohnaka and Yamashita*, 1989]

$$\dot{D}_{\max} = \frac{\Gamma\phi'_{\max}}{\pi^2}\frac{V}{C(V)}\frac{\Delta\tau_b}{\mu} \tag{24}$$

and

$$\ddot{D}_{\max} = \frac{\Gamma^2\phi''_{\max}}{\pi^4}\left(\frac{V}{C(V)}\frac{\Delta\tau_b}{\mu}\right)^2\frac{1}{D_c}, \tag{25}$$

respectively, where $\phi'_{\max}$ is the nondimensional peak slip velocity, and $\phi''_{\max}$ is the nondimensional peak slip acceleration. From equations (24) and (25), the following relation

$$\ddot{D}_{\max} = \frac{h}{D_c}\left(\dot{D}_{\max}\right)^2 \tag{26}$$

has been derived [*Ohnaka and Yamashita*, 1989], where

$$h = \frac{\phi''_{\max}}{\left(\phi'_{\max}\right)^2} \tag{27}$$

The parameter h has a value in the range 4.9–7.2 [*Ohnaka and Yamashita*, 1989], and hence h may be regarded as virtually constant.

[64] Relation (26) shows that the peak slip acceleration $\ddot{D}_{\max}$ is a function of the peak slip velocity $\dot{D}_{\max}$ and the breakdown slip displacement D_c. Figure 14 shows a plot of the logarithm of $\ddot{D}_{\max}$ against the logarithm of $\dot{D}_{\max}$. Solid lines in the figure represent theoretical relationships between $\ddot{D}_{\max}$ and $\dot{D}_{\max}$, where an amount of D_c has been specified to be 1 μm, 10 μm, 1 mm, 10 cm, 1 m, or 10 m, and where h = 5 has been assumed. Black dots in the figure denote data points obtained in the laboratory experiments on stick-slip that propagates dynamically on a precut fault of relatively large size (≈40 cm). These data were taken from an earlier paper [*Ohnaka et al.*, 1987], with additional unpublished data. One can see from Figure 14 that the peak slip acceleration for stick-slip events of laboratory-scale is very high, ranging from 10^2 to 10^5 m/s^2, while the peak slip velocity ranges from 1 to 40 cm/s. D_c for these stick-slip events in the laboratory is an independently measurable quantity, and has been found to be very small, ranging from 1 to 10 μm [*Ohnaka et al.*, 1987]. Thus, we find from Figure 14 that theoretical relation (26) very well explains those experimental data on stick-slip in quantitative terms.

[65] On the other hand, near-source strong motion records for major earthquakes have shown that the peak fault slip acceleration falls in a range from 0.5 to 5 m/s^2, and that the peak fault slip velocity falls in a range from 1 to 10 m/s. These ranges in the peak slip acceleration and velocity constrain the amount of D_c allowed for major earthquakes. It is predicted from Figure 14 that D_c should be larger than

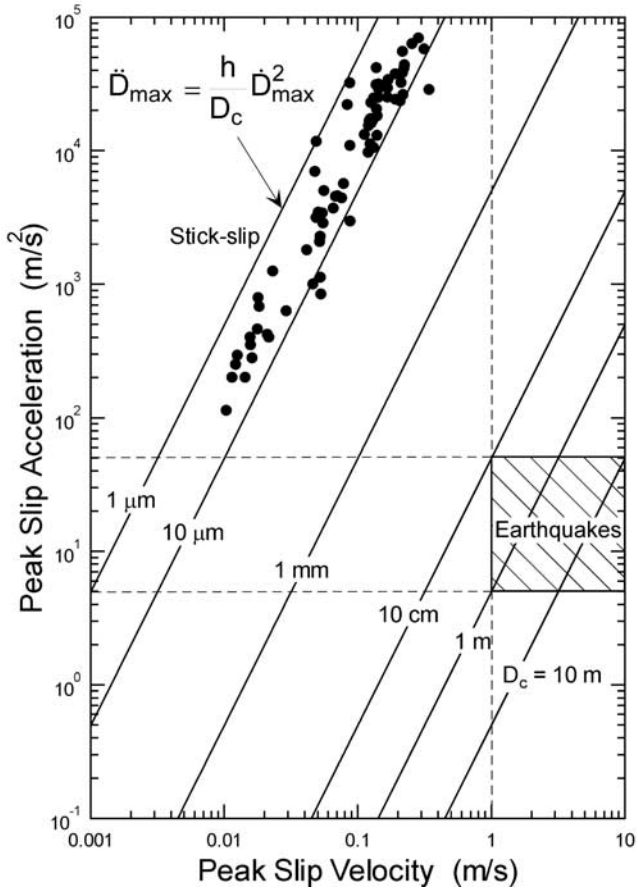

Figure 14. A plot of the logarithm of $\ddot{D}_{max}$ against the logarithm of $\dot{D}_{max}$. Black dots in the figure denote laboratory data on frictional stick-slip failure that propagates dynamically on a pre-cut fault, and solid lines represent theoretical relationships between $\ddot{D}_{max}$ and $\dot{D}_{max}$ under the assumption that D_c = 1 μm, 10 μm, 1 mm, 10 cm, 1 m, or 10 m.

10 cm for major earthquakes. Figure 14 also predicts that it is very appropriate for D_c for large earthquakes to have a value of 1 m or larger; otherwise, either $\ddot{D}_{max}$ or $\dot{D}_{max}$ is necessarily forced to have a physically unrealistic value. Let us assume for instance that D_c for major earthquakes is as small as the amount of D_c (=1–10 μm) for stick-slip events in the laboratory, and that $\ddot{D}_{max}$ is of the order of 10 m/s^2 (=1g). In this case, we have from equation (26) that $\dot{D}_{max}$ necessarily has a value as small as 1 to 10 mm/s, which is unrealistic for real, major earthquakes. If it is assumed for major earthquakes that D_c is 1–10 μm, and that $\dot{D}_{max}$ is in between 1 and 10 m/s, then it follows from equation (26) that $\ddot{D}_{max}$ necessarily has a value as large as 10^6 to 10^7 m/s^2, which is also unrealistic for major earthquakes. We thus necessarily come to the conclusion that D_c must be scale-dependent, and that D_c for large earthquakes must be on the order of 1 m, which is 3–6 orders of slip amounts larger than D_c for small-scale rupture in the laboratory.

5.2. Nucleation Zone and Breakdown Zone

[66] Recent high-resolution laboratory experiments [*Ohnaka and Shen*, 1999] have revealed the physical nature of the shear rupture nucleation that proceeds on an inhomogeneous fault. Based on findings with these high-resolution experiments, a physical model of the earthquake nucleation has been put forward to explain seismological data on the nucleation in terms of the underlying physics [*Ohnaka*, 2000]. The nucleation model proposed is reproduced in Figure 15, in which the hatched portion indicates the zone in which the breakdown (or slip-weakening) proceeds with time. In this model, the rupture nucleation initially proceeds stably and quasi-statically at a steady speed V_{st} (phase I) to a critical length $2L_{sc}$ (L_{sc}, half-length), beyond which the nucleation extends spontaneously at accelerating speeds (phase II) up to another critical length $2L_c$ (L_c, half-length) at a time $t = t_c$ in Figure 15. After the rupture growth length has reached the critical length $2L_c$, the rupture propagates at a constant, high-speed V_c close to the shear wave velocity.

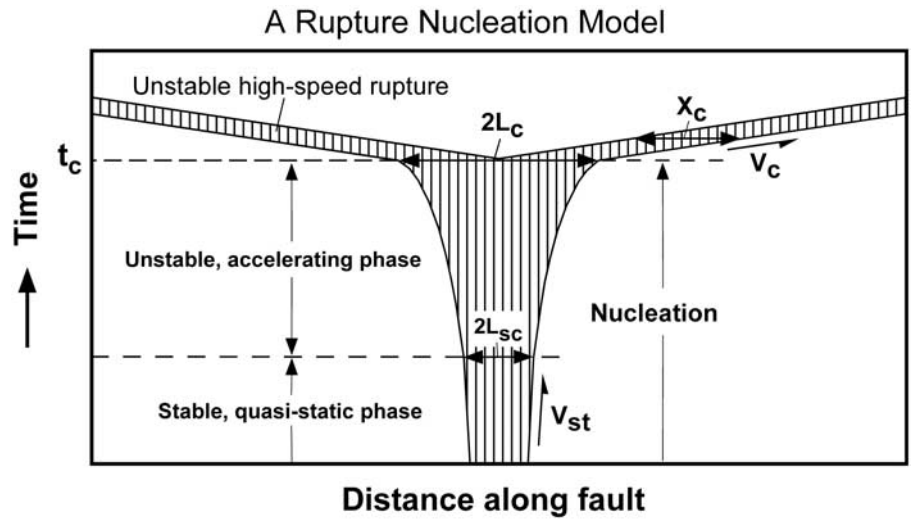

Figure 15. A physical model of rupture nucleation. Hatched portion indicates the zone in which the breakdown (or slip-weakening) proceeds with time.

[67] Phase I is a steady rupture growth controlled by the rate of an applied load, such as tectonic loading, whereas phase II is a spontaneous rupture extension driven by the release of the elastic strain energy stored in the surrounding medium. The behavior of rupture growth thus changes at the critical length $2L_{sc}$ from a quasi-static phase controlled by the applied load to a self-driven, dynamic, and accelerating phase controlled by the inertia. The behavior of rupture extension also changes at the critical length $2L_c$ from a dynamic, accelerating phase to the dynamic (virtually) terminal phase of constant high-speed rupture. The critical length of the nucleation zone is defined here not as $2L_{sc}$ but as $2L_c$, to make it possible to compare the critical size of the earthquake nucleation phase estimated from seismological data with the corresponding laboratory data on the fracture and frictional slip failure.

[68] In this model, the critical size $2L_c$ (L_c, half-length) of the nucleation zone is related to the breakdown zone size X_c in the dynamic phase of constant high-speed rupture, and L_c and X_c are expressed in terms of the constitutive parameters $\Delta\tau_b$ and D_c as follows [*Ohnaka and Shen*, 1999; *Ohnaka*, 2000]:

$$L_c = X_c = \frac{1}{k}\frac{\mu}{\Delta\tau_b}D_c \tag{28}$$

where μ is the rigidity, and k is a dimensionless parameter defined by [*Ohnaka and Yamashita*, 1989]

$$k = \frac{\Gamma}{\pi^2 \xi C(V_c)} \tag{29}$$

In equation (29), ξ represents a numerical parameter, $C(V_c)$ represents a well-defined function of the rupture velocity V_c, and Γ is a dimensionless parameter defined by equation (15). This model allows one to compare the critical size of earthquake nucleation phase or the breakdown zone size with the size of the corresponding phase for the shear fracture of intact rock and frictional slip failure in the laboratory.

[69] Equation (28) predicts that both L_c and X_c are scale-dependent, and that they should scale with D_c. In particular, L_c and X_c are directly proportional to D_c if $\Delta\tau_b$ is constant. Figure 16 shows a plot of the logarithm of L_c or X_c against the logarithm of D_c for the shear fracture of intact rock listed in Table 1, frictional slip failure listed in Tables 2 and 3, and earthquakes compiled in the earlier paper [*Ohnaka*, 2000]. In Figure 16, white squares denote data taken from *Papageorgiou and Aki* [1983], black circles denote data from *Ellsworth and Beroza* [1995], and white squares with cross denote data from *Ide and Takeo* [1997]. If $k = 3$ and μ = 30,000 MPa are assumed [see *Ohnaka*, 2000], L_c corresponding to the critical size of the earthquake nucleation phase can be estimated from equation (28) for the shear fracture of intact rock and frictional slip failure in the laboratory. The logarithm of L_c thus estimated is also plotted in Figure 16 against the logarithm of D_c for the shear fracture of intact rock samples and frictional slip failure in the laboratory for comparison. Black squares in the figure indicate data on the shear fracture of intact granite, and black and white triangles indicate data on frictional slip failure on pre-cut faults with λ_c = 200 μm and λ_c = 100 μm, respectively.

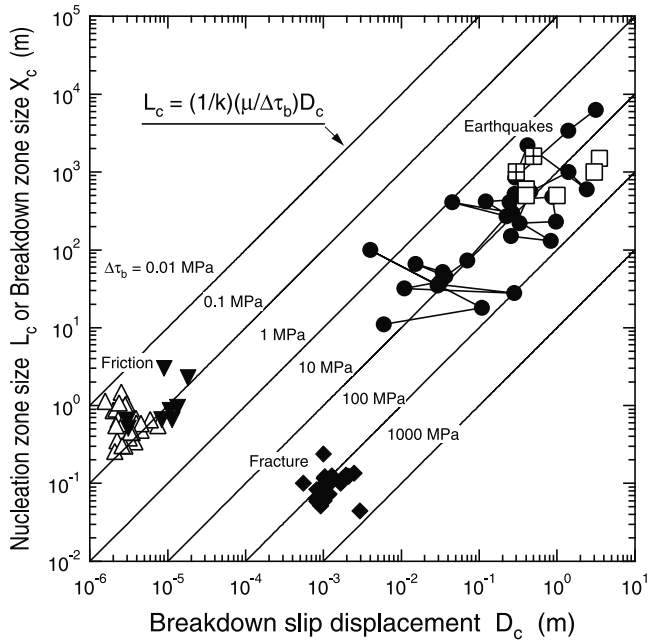

Figure 16. A plot of the logarithm of L_c or X_c against the logarithm of D_c for laboratory data on the shear fracture (Table 1) and the frictional slip failure (Tables 2 and 3), and field data on earthquake rupture. Data on earthquakes are taken from the work of *Papageorgiou and Aki* [1983], *Ellsworth and Beroza* [1995], and *Ide and Takeo* [1997]. Solid lines represent scaling relations between L_c or X_c and D_c when $\Delta\tau_b$ = 0.01, 0.1, 1, 10, 100, or 1000 MPa has been assumed.

[70] Straight lines in Figure 16 indicate proportional relationships between L_c (or X_c) and D_c derived from theoretical equation (28) under the assumption that $\Delta\tau_b$ is constant. However, the scaling relation between L_c (or X_c) and D_c is severely violated by the magnitude of $\Delta\tau_b$ because $\Delta\tau_b$ takes any value in a wide range from 1 to 100 MPa for earthquakes, depending on the seismogenic environment. Laboratory data show that $\Delta\tau_b$ has a very low value in a range from 0.01 to 0.2 MPa for frictional slip failure (Tables 2 and 3), and has a very high value in a range from 50 to 700 MPa for the shear fracture of intact rock samples (Table 1). Therefore, the effect of $\Delta\tau_b$ must be equalized when scaling relation between L_c (or X_c) and D_c for earthquakes is compared with the corresponding relations for the shear fracture of intact rock and for the frictional slip failure in the laboratory.

[71] It is estimated from equation (28) that L_c (or X_c) is roughly 10 cm or less for the shear fracture of intact rock because of a very high value for $\Delta\tau_b$. It is also estimated from equation (28) that L_c (or X_c) has a value mostly in between 20 cm and 2 m for the frictional slip failure because of a very low value for $\Delta\tau_b$, in spite of a small amount of D_c. On the other hand, L_c (or X_c) for earthquakes has been estimated to be in between 10 m and 10 km, according to the amount of D_c and the magnitude of $\Delta\tau_b$ (Table 1 of *Ohnaka* [2000], and see also Figure 16). It is found from Figure 16 that equation (28) makes it possible to unify laboratory data and field data, and to explain them consistently in quantitative terms. This also justifies the

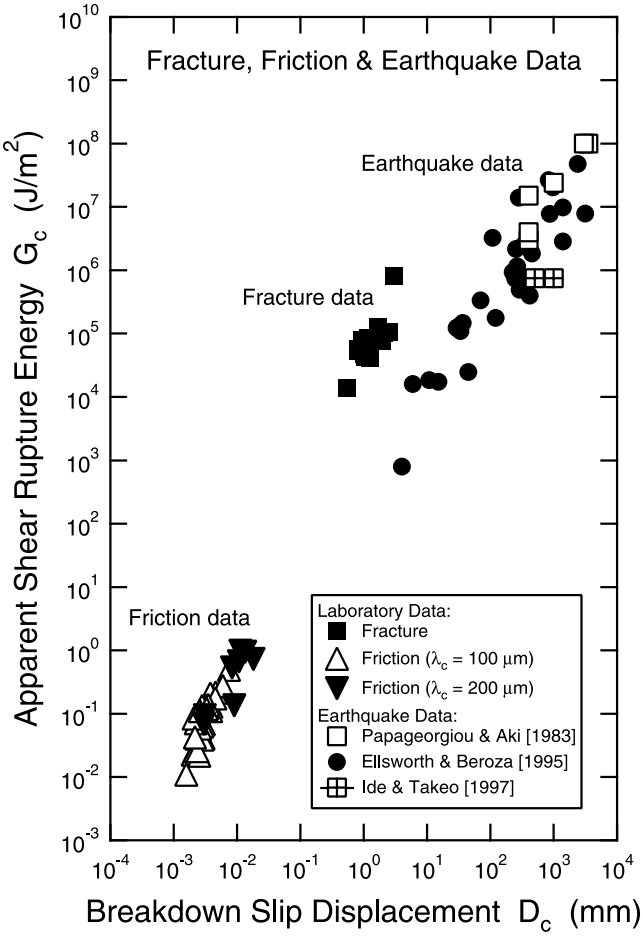

Figure 17. A plot of the logarithm of G_c against the logarithm of D_c for laboratory data on the shear fracture (Table 1) and the frictional slip failure (Tables 2 and 3), and field data on earthquake rupture.

theoretical prediction that both L_c and X_c are scale-dependent, and that L_c (or X_c) for earthquakes is much larger than that for the shear fracture of intact rock and frictional slip failure in the laboratory. A unified comprehension can thus be provided by a single scaling law of the form equation (28) for the nucleation zone size and the breakdown zone size for small-scale fracture and frictional slip failure in the laboratory and large-scale earthquake rupture in the field, despite their vast scale differences.

5.3. Apparent Shear Rupture Energy

[72] Figure 17 shows a plot of the logarithm of G_c against the logarithm of D_c for earthquakes. In Figure 17, white squares denote data on G_c estimated for earthquakes by *Papageorgiou and Aki* [1983], black circles indicate those for earthquakes analyzed by *Ellsworth and Beroza* [1995], and white squares with cross indicate those for the 1995 Kobe earthquake analyzed by *Ide and Takeo* [1997]. Since *Ellsworth and Beroza* [1995] and *Ide and Takeo* [1997] did not estimate G_c for earthquakes in their papers, G_c for these earthquakes has been evaluated in this paper from equation (14) by assuming that $\Gamma = 1$. G_c for shear fracture data listed in Table 1 and frictional slip failure data listed in Tables 2 and 3 has also been over-plotted in Figure 17 for comparison.

[73] It is found from Figure 17 that G_c increases with an increase in D_c not only for earthquake data alone but also for each set of laboratory data for the shear fracture and frictional slip failure. This is a direct manifestation of the fact that both G_c and D_c are scale-dependent. The scale-dependence of G_c is necessarily concluded from theoretical relation (14), and from the fact that D_c is scale-dependent, and that $\Delta\tau_b$ and Γ are scale-independent. As discussed in previous section, this scale-dependence is ascribed to the fact that real rupture surfaces of inhomogeneous materials are not flat plane, and that the real area of rupture surface is significantly different from the apparent area of rupture plane.

[74] One notable fact in Figure 17 is that G_c for the shear fracture of intact rock samples is 4–6 orders of magnitudes greater than G_c for the frictional slip failure. Why G_c for the shear fracture is so largely different from that for frictional slip failure has been discussed in previous section. Another notable fact is that G_c for large earthquakes is of the order of 10^7 to 10^8 J/m^2, which is 2–3 orders of magnitude greater than G_c for the shear fracture of intact rock samples tested in the laboratory. This great difference is ascribed to the scale-dependence of D_c. Indeed, D_c for large earthquakes is 2–3 orders of slip amounts greater than that for the shear fracture of intact rock samples in the laboratory.

[75] For earthquake data, both τ_p and λ_c are unknown, so that it is not possible to plot $G_c/(\tau_p\lambda_c)$ against $\Delta\tau_b/\tau_p$ or D_c/λ_c, as shown in Figure 13 for laboratory data. This does not allow one to demonstrate straightforwardly that G_c for earthquakes can be unified with laboratory data on G_c for the shear fracture of intact rock and the frictional slip failure by the law (22) or (23). Yet, it can be concluded that a law of the form (22) or (23) is necessary for unifying field data on scale-dependent G_c with the corresponding laboratory data, and that its unified comprehension is provided by equations (22) or (23), if τ_p and λ_c are suitably evaluated for earthquakes.

6. Discussion

[76] The conclusion that D_c is scale-dependent is fundamentally important because it has been shown that the scale-dependence of scale-dependent physical quantities inherent in the shear rupture is ascribed to the scale-dependence of D_c [e.g., *Ohnaka*, 1996; *Ohnaka and Shen*, 1999]. As demonstrated previously, the scale-dependent physical quantities include the slip acceleration $\dot{D}$, the breakdown zone size X_c, the nucleation zone size L_c, and the apparent shear rupture energy G_c. These scale-dependent physical quantities scale with D_c, and D_c in turn scales with the characteristic length λ_c by constitutive scaling relation (10). A large-scale fault tends to include a large, predominant wavelength component (characteristic length) of geometric irregularity of the fault surfaces, and therefore X_c, L_c, and G_c for larger earthquakes tend to have larger values in a statistical sense. Indeed, a physical scaling relation between L_c (or X_c) and the main shock seismic moment M_0 has been derived theoretically in the framework of fracture mechanics based on a laboratory-based slip-dependent constitutive law [*Ohnaka*, 2000], and it has also been shown [*Ohnaka*, 2000] that the scaling relation theoretically derived quantitatively explains seismological data analyzed by seismologists

[*Ellsworth and Beroza*, 1995; *Papageorgiou and Aki*, 1983; *Ide and Takeo*, 1997].

[77] The seismogenic layer contains a large number of preexisting faults of microscopic to macroscopic scales, and hence the seismogenic layer is inherently inhomogeneous. In addition, an individual fault in the seismogenic layer also exhibits structural inhomogeneities of various scales. Although these natural fault surfaces exhibit self-similarity over finite bandwidths [*Scholz and Aviles*, 1986; *Aviles et al.*, 1987; *Okubo and Aki*, 1987], they cannot be self-similar at all scales. The reason for this is because the shear rupture is the process that smoothes away geometric irregularity of the rupturing surfaces. In addition, the self-similarity is necessarily limited by the depth of seismogenic layer and fault segment size [e.g., *Aki*, 1984, 1992, 1996; *Knopoff*, 1996]. When the self-similarity of fault surfaces is band-limited, a characteristic length scale can be defined as the corner wavelength that separates the neighboring two bands, as noted previously. Structural inhomogeneities of a fault include fault bend or stepover, and asperities on the fault surfaces with geometric irregularity. High resistance to rupture growth will be attained at portions of fault bend or stepover, at interlocking asperities on the fault surfaces with geometric irregularity, and/or at portions of adhesion (or cohesion) healed between the mating fault surfaces during the interseismic period. The size of such a patch of high resistance to rupture growth on a fault can also be a characteristic length scale departed from the self-similarity on the fault. We can thus conclude that natural faults contain a wide range of characteristic length scales departed from the self-similarity [see also *Aki*, 1979, 1984, 1996].

[78] It has been shown from the laboratory experiments that the characteristic length scale λ_c plays a crucial role in scaling scale-dependent physical quantities inherent in the rupture. This poses a question about how large the effective characteristic length λ_c is for real earthquakes. We here infer λ_c for earthquakes under the assumption that constitutive scaling law (10) can be extrapolated to the earthquake rupture. Constitutive scaling law (10) predicts: $\lambda_c \cong 1.5\ D_c$ if $\Delta\tau_b/\tau_p = 1$, $\lambda_c \cong 10\ D_c$ if $\Delta\tau_b/\tau_p = 0.1$, $\lambda_c \cong 70\ D_c$ if $\Delta\tau_b/\tau_p = 0.01$, and $\lambda_c \cong 480\ D_c$ if $\Delta\tau_b/\tau_p = 0.001$. It can thus be concluded that λ_c is of the same order of D_c if $\Delta\tau_b/\tau_p = 1$ (complete stress drop); however, λ_c is 1–2 orders of magnitude greater than D_c if $\Delta\tau_b/\tau_p < 0.1$. For real earthquakes, it is likely that $\Delta\tau_b/\tau_p \geq 0.01$; however, it may be unrealistic to assume that $\Delta\tau_b/\tau_p < 0.01$. It will be much more unrealistic to assume that $\tau_p > 1000$ MPa at depths in the brittle seismogenic layer, because τ_p for intact rock tested at simulated crustal conditions in the laboratory does not exceed 1000 MPa.

[79] The effective characteristic length λ_c can specifically be inferred for earthquakes for which the constitutive law parameters $\Delta\tau_b$ and D_c have been estimated, if τ_p is appropriately assumed. For instance, if $\tau_p = 100$ MPa is assumed for Californian earthquakes analyzed by *Papageorgiou and Aki* [1983], and *Ellsworth and Beroza* [1995], then λ_c/D_c has a value ranging from 1.5 to 150, depending on a specific value for $\Delta\tau_b/\tau_p$. Figure 18 shows a plot of the logarithm of D_c against the logarithm of λ_c for laboratory data on the shear fracture of intact rock (Table 1) and frictional slip failure (Tables 2 and 3), and field data on earthquake rupture compiled in Table 1 in *Ohnaka* [2000].

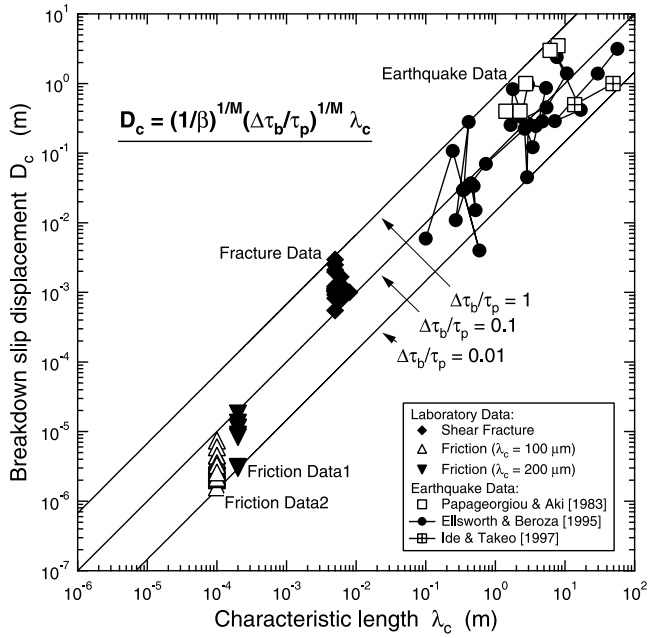

Figure 18. A plot of the logarithm of D_c against the logarithm of λ_c for laboratory data on the shear fracture (Table 1) and the frictional slip failure (Tables 2 and 3), and field data on earthquake rupture. Solid lines represent constitutive scaling relations between D_c and λ_c when $\Delta\tau_b/\tau_p = 0.01$, 0.1, or 1 has been assumed.

In this plot, the peak shear strength τ_p for earthquakes has been assumed to be 100 MPa. If τ_p for these earthquakes is higher than 100 MPa, data points for the earthquakes shift rightward in Figure 18, and if τ_p for those earthquakes is lower than 100 MPa, data points for the earthquakes shift leftward in Figure 18, with the constraint that $\Delta\tau_b/\tau_p \leq 1$. Solid straight lines in the figure represent constitutive scaling relations between D_c and λ_c for the three cases where $\Delta\tau_b/\tau_p$ has been assumed to be 0.01, 0.1, and 1. It is clearly seen from Figure 18 that D_c has different values according to specific values of λ_c, and this requires a scaling relation for a consistent and unified comprehension even for laboratory data alone.

[80] We here consider a specific case where $D_c = 1$ m, $\Delta\tau_b = 10$ MPa, and $\tau_p = 100$ MPa, which may be regarded as a representative case for large earthquakes. In this case, the effective characteristic length λ_c has a value of 10 m. If $k = 3$ and $\mu = 30{,}000$ MPa are further assumed [see *Ohnaka*, 2000], we have from equation (28) that the breakdown zone size X_c is 1 km. This means that a predominant wavelength component of 10 m is contained in geometric irregularity of the rupture surfaces over the breakdown zone distance of 1 km. This may be paraphrased as follows. Under the stress condition that $\Delta\tau_b/\tau_p = 0.1$, the amount of 1 m for D_c is required for breaking down the cohesive zone size of 1 km, and the rupture surfaces newly created have geometric irregularity characterized by a predominant wavelength component of 10 m. It will not be unreasonable to postulate that the characteristic length of 10 m is contained in geometric irregularity of the rupture surfaces over the distance of 1 km.

[81] Thus, a consistent and unified comprehension can be provided for small–scale frictional slip failure and shear

fracture in the laboratory, and large-scale earthquake rupture in the field if a constitutive scaling law of the form (10) is assumed for earthquake rupture.

7. Conclusions

[82] It has been explored how laboratory data on both frictional slip failure and shear fracture of intact rock, and field data on earthquake rupture can be unified consistently by a single constitutive law. Noting that the earthquake rupture on an inhomogenous fault is a mixed process between frictional slip failure and the shear fracture of intact rock, it has been concluded that the constitutive law for the earthquake rupture should be formulated as a unifying law that governs both frictional slip failure and shear fracture of intact rock. The slip-dependent constitutive law is a unifying law that governs both frictional slip failure and shear fracture of intact rock. A constitutive scaling law formulated by equations (10) and (11), has been derived from laboratory data on both frictional slip failure and shear fracture of intact rock. This constitutive scaling law enables one to provide a consistent, unified comprehension for small-scale frictional slip failure and shear fracture in the laboratory, and large-scale earthquake rupture in the field. Real, irregular rupture surfaces have characteristic length scales departed from self-similarity, and the effective characteristic length λ_c is a parameter representing the geometric irregularity of the rupture surfaces. The breakdown slip displacement D_c scales with λ_c, and this scaling relation can be violated by the magnitude of $\Delta\tau_b/\tau_p$. The rupture energy G_c is not only dependent on the material property, but also related to the real area of geometrically irregular rupture surfaces. Hence G_c is necessarily scale-dependent; however, this scale dependence can be violated by the magnitudes of τ_p and $\Delta\tau_b$, because G_c is expressed by equation (20) in terms of τ_p, $\Delta\tau_b$ and λ_c, or equivalently (21) in terms of τ_p, D_c and λ_c. Since $\ddot{D}$, L_c, and X_c scale with D_c, these scale-dependent physical quantities also scale with λ_c. It has been inferred for earthquakes that the ratio λ_c/D_c has a value ranging from 1.5 to 480, according to the magnitude of $\Delta\tau_b/\tau_p$. The present studies logically lead to the consistent conclusion that D_c is scale-dependent, and that D_c for large earthquakes must be as large as the order of 1 m, which agrees with values for D_c estimated for large earthquakes by seismologists.

[83] **Acknowledgments.** A great number of elaborate laboratory experiments have been performed to obtain a series of data used in this paper, and H. Mochizuki, L.-F. Shen, and A. Odedra took part in this series of laboratory experiments. I am very grateful to them for joining in a stage of the present series of laboratory work. I am also very grateful to Ian Main and an anonymous reviewer for reviewing the original manuscript, whose thoughtful comments contributed to enhancing the value of the paper.

References

Aki, K., Characterization of barriers on an earthquake fault, *J. Geophys. Res.*, *84*, 6140–6148, 1979.

Aki, K., Asperities, barriers, characteristic earthquakes and strong motion prediction, *J. Geophys. Res.*, *89*, 5867–5872, 1984.

Aki, K., Higher-order interrelations between seismogenic structures and earthquake processes, *Tectonophysics*, *211*, 1–12, 1992.

Aki, K., Scale dependence in earthquake phenomena and its relevance to earthquake prediction, *Proc. Natl. Acad. Sci. U. S. A.*, *93*, 3740–3747, 1996.

Aviles, C. A., C. H. Scholz, and J. Boatwright, Fractal analysis applied to characteristic segments of the San Andreas fault, *J. Geophys. Res.*, *92*, 331–344, 1987.

Beroza, G. C., and T. Mikumo, Short slip duration in dynamic rupture in the presence of heterogeneous fault properties, *J. Geophys. Res.*, *101*, 22,449–22,460, 1996.

Bouchon, M., The state of stress on some faults of the San Andreas system as inferred from near-field strong motion data, *J. Geophys. Res.*, *102*, 11,731–11,744, 1997.

Day, S. M., G. Yu, and D. J. Wald, Dynamic stress changes during earthquake rupture, *Bull. Seismol. Soc. Am.*, *88*, 512–522, 1998.

Dieterich, J. H., Preseismic fault slip and earthquake prediction, *J. Geophys. Res.*, *83*, 3940–3948, 1978.

Dieterich, J. H., Modeling of rock friction, 1, Experimental results and constitutive equations, *J. Geophys. Res.*, *84*, 2161–2168, 1979.

Dieterich, J. H., Constitutive properties of faults with simulated gouge, in *Mechanical Behavior of Crustal Rocks*, *Geophys. Monogr. Ser.*, vol. 24, edited by N. L. Carter et al., pp. 102–120, AGU, Washington, D. C., 1981.

Dieterich, J. H., A model for the nucleation of earthquake slip, in *Earthquake Source Mechanics, Geophys. Monogr. Ser.*, vol. 37, edited by S. Das, J. Boatwright, and C. H. Scholz, pp. 37–47, AGU, Washington, D. C., 1986.

Ellsworth, W. L., and G. C. Beroza, Seismic evidence for an earthquake nucleation phase, *Science*, *268*, 851–855, 1995.

Ida, Y., Cohesive force across the tip of a longitudinal-shear crack and Griffith's specific surface energy, *J. Geophys. Res.*, *77*, 3796–3805, 1972.

Ida, Y., The maximum acceleration of seismic ground motion, *Bull. Seismol. Soc. Am.*, *63*, 959–968, 1973.

Ide, S., and M. Takeo, Determination of constitutive relations of fault slip based on seismic wave analysis, *J. Geophys. Res.*, *102*, 27,379–27,391, 1997.

Kanamori, H., The nature of seismic patterns before large earthquakes, in *Earthquake Prediction: An International Review*, edited by D. W. Simpson and P. G. Richards, pp. 1–19, AGU, Washington, D. C., 1981.

Kanamori, H., and G. S. Stewart, Seismological aspects of the Guatemala earthquake of February 4, 1976, *J. Geophys. Res.*, *83*, 3427–3434, 1978.

Kato, A., H. Mochizuki, S. Yoshida, and M. Ohnaka, Strain rate dependence of constitutive properties for the shear failure of intact rock in seismogenic environments, paper presented at Fall Meeting of Seismological Society of Japan, Kagoshima, *Prog. Abstr.*, A28, 2001.

Kato, A., M. Ohnaka, and H. Mochizuki, Constitutive properties for the shear failure of intact granite in seismogenic environments, *J. Geophys. Res.*, 10.1029/2001JB000791, in press, 2002.

Knopoff, L., The organization of seismicity on fault networks, *Proc. Natl. Acad. Sci. U. S. A.*, *93*, 3830–3837, 1996.

Matsu'ura, M., H. Kataoka, and B. Shibazaki, Slip-dependent friction law and nucleation processes in earthquake rupture, *Tectonophysics*, *211*, 135–148, 1992.

Odedra, A., Laboratory studies on shear fracture of granite under simulated crustal conditions, Ph.D. thesis, pp. 1–269, Univ. College London, London, 1998.

Odedra, A., M. Ohnaka, H. Mochizuki, and P. Sammonds, Temperature and pore pressure effects on the strength of granite in the brittle-plastic transition regime, *Geophys. Res. Lett.*, *28*, 3011–3014, 2001.

Ohnaka, M., Earthquake source nucleation: A physical model for short-term precursors, *Tectonophysics*, *211*, 149–178, 1992.

Ohnaka, M., Nonuniformity of the constitutive law parameters for shear rupture and quasistatic nucleation to dynamic rupture: A physical model of earthquake generation processes, *Proc. Natl. Acad. Sci. U. S. A.*, *93*, 3795–3802, 1996.

Ohnaka, M., A physical scaling relation between the size of an earthquake and its nucleation zone size, *Pure Appl. Geophys.*, *157*, 2259–2282, 2000.

Ohnaka, M., and L. F. Shen, Scaling of the shear rupture process from nucleation to dynamic propagation: Implications of geometric irregularity of the rupturing surfaces, *J. Geophys. Res.*, *104*, 817–844, 1999.

Ohnaka, M., and T. Yamashita, A cohesive zone model for dynamic shear faulting based on experimentally inferred constitutive relation and strong motion source parameters, *J. Geophys. Res.*, *94*, 4089–4104, 1989.

Ohnaka, M., Y. Kuwahara, and K. Yamamoto, Constitutive relations between dynamic physical parameters near a tip of the propagating slip zone during stick-slip shear failure, *Tectonophysics*, *144*, 109–125, 1987.

Ohnaka, M., M. Akatsu, H. Mochizuki, A. Odedra, F. Tagashira, and Y. Yamamoto, A constitutive law for the shear failure of rock under lithospheric conditions, *Tectonophysics*, *277*, 1–27, 1997.

Okubo, P. G., and K. Aki, Fractal geometry in the San Andreas fault system, *J. Geophys. Res.*, *92*, 345–355, 1987.

Okubo, P. G., and J. H. Dieterich, State variable fault constitutive relations for dynamic slip, in *Earthquake Source Mechanics, Geophys. Monogr. Ser.*, vol. 37, edited by S. Das, J. Boatwright, and C. H. Scholz, pp. 25–35, AGU, Washington, D. C., 1986.

Palmer, A. C., and J. R. Rice, The growth of slip surfaces in the progressive failure of over-consolidated clay, *Proc. R. Soc. London, Ser. A.*, *332*, 527–548, 1973.

Papageorgiou, A. S., and K. Aki, A specific barrier model for the quantitative description of inhomogeneous faulting and the prediction of strong ground motion, part II, Applications of the model, *Bull. Seismol. Soc. Am.*, *73*, 953–978, 1983.

Rice, J. R., The mechanics of earthquake rupture, in *Physics of the Earth's Interior, Proc. Int. Sch. Phys. Enrico Fermi*, edited by A. M. Dziewonski and E. Boschi, pp. 555–649, North-Holland, New York, 1980.

Ruina, A., Slip instability and state variable friction laws, *J. Geophys. Res.*, *88*, 10,359–10,370, 1983.

Ruina, A. L., Constitutive relations for frictional slip, in *Mechanics of Geomaterials*, edited by Z. Bazant, pp. 169–188, John Wiley, New York, 1985.

Scholz, C. H., and C. A. Aviles, The fractal geometry of faults and faulting, in *Earthquake Source Mechanics, Geophys. Monogr. Ser.*, vol. 37, edited by S. Das, J. Boatwright, and C. H. Scholz, pp. 147–155, AGU, Washington, D. C., 1986.

Wong, T.-F., Shear fracture energy of Westerly granite from post-failure behavior, *J. Geophys. Res.*, *87*, 990–1000, 1982a.

Wong, T.-F., Effects of temperature and pressure on failure and post-failure behavior of Westerly granite, *Mech. Mater.*, *1*, 3–17, 1982b.

Wong, T.-F., On the normal stress dependence of the shear fracture energy, in *Earthquake Source Mechanics*, *Geophys. Monogr. Ser.*, vol. 37, edited by S. Das, J. Boatwright, and C. H. Scholz, pp. 1–11, AGU, Washington, D. C., 1986.

York, D., Least-squares fitting of a straight line, *Can. J. Phys.*, *44*, 1079–1086, 1966.

M. Ohnaka, Utsukushigaoka-Nishi 3-40-19, Aoba-ku, Yokohama 225-0001, Japan. (ohnaka-m@eri.u-tokyo.ac.jp; ohnaka@fd.catv.ne.jp)